Arabian Journal of Chemistry (2023) **16**, 104997

King Saud University

Arabian Journal of Chemistry

www.ksu.edu.sa
www.sciencedirect.com

REVIEW ARTICLE

Morphology-controllable bimetallic gold nanostructures for mercury detection: Recent developments, challenges and prospects

Shujat Ali [a], Xi Chen [a], Shujaat Ahmad [b], Mazen Almehmadi [c], Ahad Amer Alsaiari [c], Mamdouh Allahyani [c], Zarif Gul [d], Abid Ullah [b], Haya Hussain [b], Limin Li [a,*], Xiaojing Chen [a,*]

[a] *College of Electrical and Electronic Engineering, Wenzhou University, Wenzhou 325035, PR China*
[b] *Department of Pharmacy Shaheed Benazir Bhutto University, Sheringal, Dir Upper, Pakistan*
[c] *Department of Clinical Laboratory Sciences, College of Applied Medical Sciences, Taif University, P.O. Box 11099, Taif 21944, Saudi Arabia*
[d] *Department of Chemistry, University of Okara, Okara, Pakistan*

Received 22 January 2023; accepted 10 May 2023
Available online 16 May 2023

KEYWORDS

Mercury detection;
Gold bimetallic nanostructure;
Morphology-controlled preparation;
Shape/size and sensing;
Nano-sensors for Hg

Abstract Gold bimetallic nanostructures (AuBMNS) have exhibited superior Hg sensing activity as compared to their monometallic counterparts. Moreover, the Hg sensing performance of AuBMNS depends on their shape, size, composition, and surface chemistry. Thus, morphology-controlled preparation and application of these nanostructures in Hg detection is a hot area of research. Till now, no review paper in the literature accounts for the recent advances in the morphology-controlled synthesis of AuBMNS and their application in sensing Hg related to shape, size, optimum composition, morphology, and surface ligands. Taking this into consideration, we attempt to offer a clear understanding of the shape/size-controlled preparation, functionalization, and morphology-dependent application of AuBMNS in Hg detection. The chemical reduction approach for the morphology-controlled preparation of AuBMNS is critically discussed. The prospective role of different reaction parameters such as temperature, pH, time, reducing agents, nature/concentration of precursors, and capping/stabilizing agents in the morphology-controlled preparation of these nanostructures are reviewed. Moreover, morphology-dependent optical properties and performance of AuBMNS are discussed with recent (2020–2022) examples. In the later

* Corresponding authors at: Building 1, North Campus, Wenzhou University, Chashan University Town, Wenzhou City, Zhejiang Province 325035, China.
E-mail addresses: lilimin@wzu.edu.cn (L. Li), chenxj@wzu.edu.cn (X. Chen).
Peer review under responsibility of King Saud University.

Production and hosting by Elsevier

https://doi.org/10.1016/j.arabjc.2023.104997

part, detection of Hg by using AuBMNS is reviewed and the effects of size, shape, surface chemistry/structure, optimum composition, and synergism are discussed. Finally, recent challenges in morphology-controlled preparation of AuBMNS, their shape/size-dependent performance, and prospects to resolve the related issues are discussed.

1. Introduction

Mercury (Hg) above a threshold limit is harmful to humans and accountable for several life-threatening illnesses (Wang et al., 2022a, 2022b, 2022c, 2022d, 2022e). Delay in the estimation and detection of Hg have been the cause of different health issues in humans (Basu et al., 2022). Hence, there is a great need to precisely and timely monitor Hg in environmental and food samples. In this regard, several chemical, biological and physical methods have been applied for Hg detection (Ali et al., 2022). However, these methods have the limitation of long pre-concentration steps, complex and lengthy protocols, costly and complicated instrumentation (Amico et al., 2022). Hence, the establishment of facile, feasible, cost-effective and rapid approaches for Hg detection is a hot area of research.

Hg contaminants are found in air, soil and water, and can enter the human body by different ways such as air, food and water (Wang et al., 2021a, 2021b, Teng and Altaf 2022). Inorganic Hg^{2+} in the atmosphere change into organic lipophilic compounds such as methylmercury (Basu et al., 2022), which gathers in meat and vegetables, and enters the human body by eating fish, causing numerous diseases (Li et al., 2022a, 2022b) (Amico et al., 2022, Árvay et al., 2022). Hence, this has been associated with the progression and/or development of neurodegenerative disorders such as Alzheimer's, Amyotrophic, Parkinson's, and Lateral Sclerosis Disorders (LSD). However, their precise role as an exacerbating or causative factor remains to be fully clarified (Azar et al., 2021, Rehman et al., 2021, Ullah et al., 2021). The need for the development of new approaches to monitor Hg contamination and to improve environmental awareness among people is necessary. Nanotechnology-based methods have been developed for easier and simpler detection of Hg contamination in environmental and food samples. Recently, gold bimetallic nanostructures (AuBMNS)-based sensors for selective and sensitive detection of Hg have been established.

Nanotechnology has presented a remarkable breakthrough with the improvement of several nano-sensors for Hg detection (Liu et al., 2022a, Shrivastava et al., 2022). Nanoparticles (NPs), with minuscule size and high surface area, have overlooked the field of detection and sensing, and have offered auspicious sensing systems (by applying feasible on-site detection) compared to the traditionally used methods (Khani et al., 2022). Particularly, gold nanoparticle (AuNPs) mediated detection systems have been of prodigious research significance as they have feasible pertinency in Hg detection (Hyder et al., 2022). Moreover, the unique optical properties and greater surface area of AuNPs help in the highly selective and sensitive detection of Hg (Zhou et al., 2022). The physiological and morphological characteristics of AuNPs greatly depend on their aggregation state, shape and size which can be fine-tuned by selecting the suitable synthesis method and stabilization agents as well as other parameters (Li et al., 2021a, Li et al., 2021b, Li et al., 2022a, 2022b). Interestingly, the addition of second/third metals (bi/trimetallic NPs) has exhibited superior detection properties as compared to their monometallic counterparts (Pandey et al., 2021, Wang et al., 2022a, 2022b, 2022c, 2022d, 2022e).

In recent years, there has been a rush of interest in the synthesis and fabrication of Au and/or Ag NPs for their prospective applications in chemical and biological sensing. Several review papers (Chatterjee et al., 2022, Gul et al., 2022, Lu 2022, Mehta et al., 2022, Xie et al., 2022) have explored the versatility of such NPs as reliable sensing agents for examining environmental and biological samples. Currently, a great contribution of heavy metal ions has been noticed towards environmental pollution and food toxicity (Mitra et al., 2022, Oladoye et al., 2022). Among these, Hg has emerged as a significant cause of environmental and food contamination (Cossa et al., 2022, Li et al., 2022a, 2022b). Interestingly, Au-based multi-metallic NPs have been reported as auspicious substrates for Hg detection as compared to their monometallic counterparts (Wang et al., 2022a, 2022b, 2022c, 2022d, 2022e). By evaluating the role of AuBMNS as admirable materials in heavy metal detection, we tried to focus our study completely on the use of these NPs in Hg detection.

Over the years, several review articles have comprehensively investigated the use of both monometallic and multi-metallic Au NPs in the detection of different organic and inorganic contaminants, along with heavy metal ions. These articles have particularly focused on the utilization of such NPs in different detection approaches such as electrochemical, fluorescent and colorimetric techniques (Hlaváček et al., 2022, Hyder et al., 2022, Mukunzi et al., 2022, Wang et al., 2022a, 2022b, 2022c, 2022d, 2022e, Zhao et al., 2022). However, the shape and size-controlled preparation of multi-metallic AuNPs, their morphology-dependent optical properties, shape/size and composition-dependent application towards Hg detection, and recent challenges and prospects are not yet reviewed. In this article, a categorical investigation of size/shape-controlled preparation of AuBMNS, their application in the detection of Hg below the threshold limit, comparative evaluation of different sensing methods (such as colorimetric, SERS, electrochemical, fluorescence, dual/combined techniques), and important challenges and prospects have been discussed. Furthermore, we analyzed the role of capping and stabilizing agents on the performance of the AuBMNS towards Hg detection. Additionally, major improvements and recent advances in designing AuBMNS of various architectures and their comparative effectiveness have also been reviewed to comprehend the recent scenario and offer upcoming directions for the sensing of Hg. Thus, the principal aim of this review paper is to focus on the latest developments and recent state-of-art of morphology-controlled preparation, functionalization and characterization of AuBMNS, and their shape/size-dependent optical, sensing properties (based on different techniques) towards Hg detection, as shown in Fig. 1.

2. Synthesis of AuBMNS with controllable shape and size

In recent years, the synthesis of gold NPs and their application in Hg detection have garnered substantial attention owing to their unique optical properties. A literature survey applying the keywords "gold nanoparticles and mercury detection" is presented in Fig. 2**(A).** The graph represents the number of articles published in the last five years (2018–2022). A gradual increase (every year) in the number of reports signifying the need for Hg determination and applying stress upon the importance of the research topic.

For AuBMNS, different methods have been applied such hydrothermal (Huang et al., 2021a), biogenic (Akilandaeaswari and Muthu 2021), seed-mediated (Zhang et al., 2019), thermolysis (Pawar et al., 2019), galvanic replacement (Chen et al., 2020), multi-step synthesis (Lu et al., 2018),

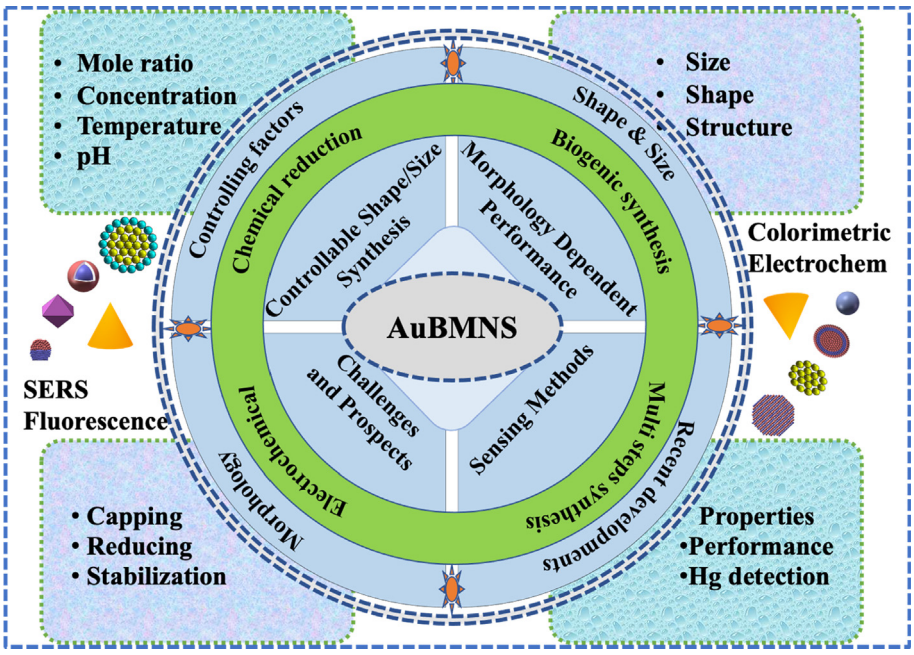

Fig. 1 Schematic demonstration of the controllable synthesis of AuBMNS and their application in Hg detection. The chemical reduction approach with the impacts of different reaction parameters have been discussed for the morphology-controlled synthesis of AuBMNS. Recent examples of AuBMNS for Hg detection have been reviewed. Challenges and prospects are discussed for future research.

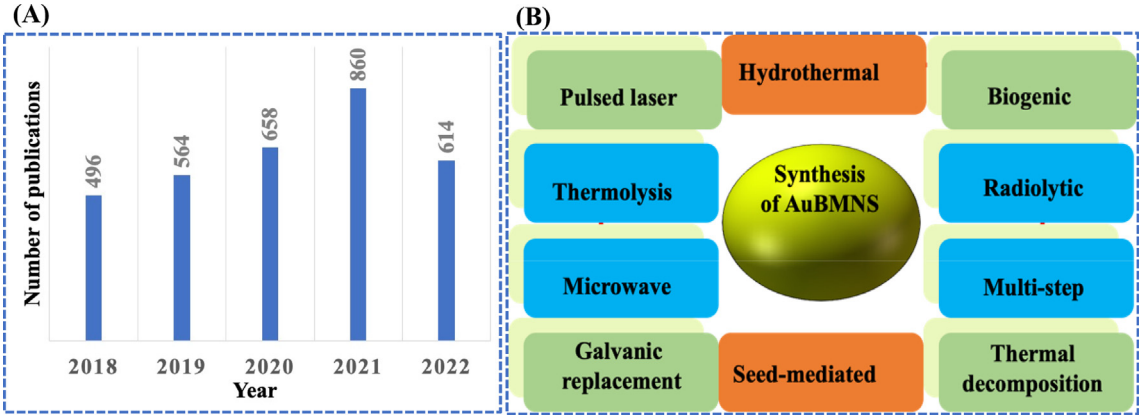

Fig. 2 **(A)** AuBMNS for Hg^{+2} detection. Number of articles in the last five years (2018–2022), searched on May 26, 2022, using the keywords "gold nanoparticles and mercury detection". **(B)** Different methods for the preparation of AuBMNS.

pulsed laser synthesis (Subhan et al., 2022), thermal decomposition (Boeva et al., 2022), microwave (Al-Radadi 2022) and radiolytic synthesis (Fernandes et al., 2021) (Fig. 2**(B)**). Furthermore, the shape, size and stability of AuBMNS change by varying the experimental parameters and preparation procedure. Based on previous reports, the chemical reduction is a suitable and extensively used method for controlling the shape, size and stability of the AuBMNS **(**Table 1**).**

In this article, we don't demonstrate a full catalog of all the methods that have been applied for the preparation of monometallic and multi-metallic Au NPs. Interesting readers are referred to some review papers dedicated to the preparation of mono-metallic and multi-metallic NPs (constituted of different types of metals) (Ali et al., 2021a, 2021b, 2021c, Saha et al., 2021, Sayadi et al., 2021, Crawley et al., 2022, Gebre 2022). Here, we only focus on the shape/size-controlled preparation of AuBMNS and their morphology-dependent application in Hg detection as well as the recent prospects and challenges.

Exact control over the synthesis procedure is required to obtain the desired shape, size and morphology of AuBMNS. Similarly, the surface functionality, structure and chemistry of AuBMNS can be tuned by regulating the reaction parameters. Moreover, nucleation and growth phases play a dynamic part in controlling the particle shape and composition. However, controlling reaction conditions in the early stages is hard and the mechanisms of morphology-controlled synthesis of AuBMNS are still under investigation (Kluitmann et al.,

Table 1 Selected examples of AuBMNS-based sensors for Hg detection.

S. No.	Type of AuBMNS	Method of preparation	Shape	Size	Functionalization	Ref.
1	Au@Fe	Chemical reduction	Spherical	85.22 nm	Ag iodide supported on polyglycine	(Liu et al., 2022a, 2022b)
2	Au@Ag core–shell	Seed-mediated route	Rod-shaped	16 nm	Chitosan modified	(Zhang et al., 2019)
3	Au@Ag hollow nanostructures	Galvanic etching	Spherical	54–75 nm	Template Ag NPs	(Jain and Satija 2018)
4	BSA-protectedAg@U NPs	Chemical reduction	Spherical	2.3 nm	BSA-protected TEA co-reduction	(Zhai et al., 2017)
5	Lysine-capedAg@Au NPs	Chemical reduction	Spherical	55 nm	Lysine-caped	(Bi et al., 2021)
6	Ag@Au NPS	Chemical reduction	Pointed tips structure	26–59 nm	AA and CTAB functionalized	(Xing et al., 2018)
7	Ag@Au Nanoclusters	Chemical reduction	Spherical	3 nm	BSA functionalized	(Liu et al., 2020)
8	Ag@Au Alloy NPs	Thermolysis	Micro-flower	30–50 μm	Tetraoctylammonium bromide (ToABr) modified	(Pawar et al., 2019)
9	Au@AgHollow nanocages	Galvanic replacement reaction	Hollow center and pinholes	100 nm	Ag nano-cubes sacrificial templates	(Chen et al., 2020)
10	Ag@AuNanocluster	One-step green method	Irregular shape	5 nm	BSA protected	(Dai et al., 2018)
11	Au@SiO_2Core-shell NPs	Pre-formed AuNPs and SiO_2	Core-shell	15 nm	Amino-Modified Au@SiO2	(Zhu et al., 2018)
12	Au-Ag core–shell triangular nanoplates	Pre-formed Au nanopaltes as tempelate	core–shell triangular nanoplates	122–142 nm	CTAB modified	(Zhu et al., 2019)
13	Au@SiO_2 core–shell NPs	Multi-step synthesis method	Spherical core–shell	120 nm	DNA aptamer-modified	(Lu et al., 2018)
14	AuNCs-Ag@Keratin	Chemical reduction	Irregular	2.63	Modification with Ag(I) ion	(Wang et al., 2018)
15	Au@S-C_3N_4	Chemical reduction	Folded sheet-like structures	30 nm	Chitosan functionalized	(Amanulla et al., 2019)
16	Fe_3O_4@Au Core-shell NPs	Chemical reduction	Spherical core–shell	80 nm	Thymine acetic acid anchored with cysteamine-conjugated	(Butmee et al., 2021)
17	Au-Pt@C Nanofiber	Hydrothermal method and electrodeposition	Fiber	400 nm	Aptamer modified	(Xie et al., 2021)
17	Ag@AuHollow nanostructures	Reduction/ heteroepitaxial seed-mediated	Spherical	26 nm	SDS capped	(Jain et al., 2020)
18	Ag@Au NPs	Chemical reduction	Spherical	28 nm	Poly(diallyl dimethyl ammonium chloride) modified	(Mathaweesansurn et al., 2020)
19	Ag-coated AuNPs	two-step reduction method	Core-shell	19 nm	agar-stabilized	(Da et al., 2018)
20	A@C_3N_4 Nanocomposites	Chemical reduction	Layered/nanosheets	100 nm	Graphite-C_3N_4 nanosheets supported	(Wang et al., 2019)
21	Ag@AuCore-shell NPs	One-pot reduction approach	Spherical	43 nm	Nafion stabilized l-cysteine-capped	(Siddiqui et al., 2019)
22	Au@Pd NPs	Chemical reduction	Irregularspherical	110 nm	Au modified thiol graphene	(Wang et al., 2022a, 2022b, 2022c, 2022d, 2022e)
23	Au@Cu nanoclusters	Chemical reduction	Spherical	3.5 nm	Aptamer-modified	(Shi et al., 2021)
24	Ag@Au NPs	Hydrothermal method	Cubic	20 nm	Zeolitic imidazolate framework	(Salandari-Jolge et al., 2021)
25	Ag@Au NPs	Green method	Spherical	5–45 nm	Extract of chlorella acidophile	(Thangaswamy et al., 2021)

2021). Moreover, it is tough to guess which reaction parameters control the size, shape, morphology and functionality of the AuBMNS (Ramos and Regulacio 2021).

The current innovations in the instrumentations for characterizing NPs have helped researchers to prepare AuBMNS with desired morphologies and compositions (Deng et al., 2021a). Nevertheless, the ideal pertinence of AuBMNS is still in the early stage to substitute the normal practices (Vilímová and Šišková 2021). Additionally, reports dealing with the morphology- and size-selective synthesis of NPs are widely available in the literature, but activity-based synthesis needs further study.

Various approaches have been developed to prepare AuBMNS with preferred shape/size and morphologies. To study all these strategies is beyond the domain of this review, here, significant parameters for regulating the size, shape and morphology of AuBMNS are described **(**Fig. 3**)**.

2.1. Reaction pH

By regulating the pH of a reaction, AuBMNS with selected structures can be prepared. Usually, at low pH, the power of a reducing agent decreases, slowing the growth rate and thus shape/size and morphology of AuBMNS can be regulated. Similarly, the size of AuBMNS decreases at a higher pH and this is associated with the reducing power of the reductant (Hammami and Alabdallah 2021). Moreover, high pH results in a greater number of nuclei at the start of a reaction and thus causes a reduction in NPs size. Occasionally, unexpected molecules and byproducts may cause alteration in reaction conditions and so change the pH of the reaction mixture. Thus, while controlling the pH of a reaction, other reaction conditions should be carefully considered. Normally, the basic condition is somewhat appropriate for the reduction of metal ions since the power of reductants increases in the presence of hydroxide ions (OH^-) (Irfan et al., 2022). In a study, AuBMNS were prepared by increasing the pH of the reaction mixture, by adding a small amount of ascorbic acid, AuBMNS with small tips and two surface plasmon resonance (SPR) modes were obtained. This was attributed to the different core and shell (metals) ratios, which were due to the enhanced de-alloying rate of the shell and the low cavitating rate of the core at high pH conditions (Xing et al., 2018). For example, in the biological synthesis of NPs, a basic medium supports the reduction of metal ions and creates NPs, hence, NPs form at a faster rate at a higher pH (Khalil et al., 2012). Furthermore, alkalinity can bring an electrostatic repulsion force among the NPs, hence, successfully inhibiting them from aggregation. Nevertheless, low pH causes a very high-positive charge on the reductants and decreases the stability of NPs, and ultimately, accumulation occurs (Shah et al., 2014).

2.2. Amount/nature of stabilizing agents

Stabilizing/capping agents can precisely interact with the AuBMNS to minimize their surface energy. These stabilizing molecules chemisorb on the surface of AuBMNS, hinder or prevent the deposition of more metallic atoms, keep a firm formation and stop the accumulation of AuBMNS (Khalaf et al., 2021). The physiochemical structure of AuBMNS mainly depends on the nature/amount of capping agent which is chemisorbed on their surface. Therefore, appropriate stabilizing agents are applied to control the size of AuBMNS and prevent their overgrowth (Khan et al., 2020). Luckily, various compounds are available as capping/stabilizing agents for the preparation of AuBMNS.

The reaction of capping molecules and AuBMNS surface depend on numerous features including functional group(s) of capping agents and surface chemistry and morphology of AuBMNS. Computational and experimental data can be applied to determine the role of a certain stabilizing agent and to figure out a specific capping agent for AuBMNS. Pre-

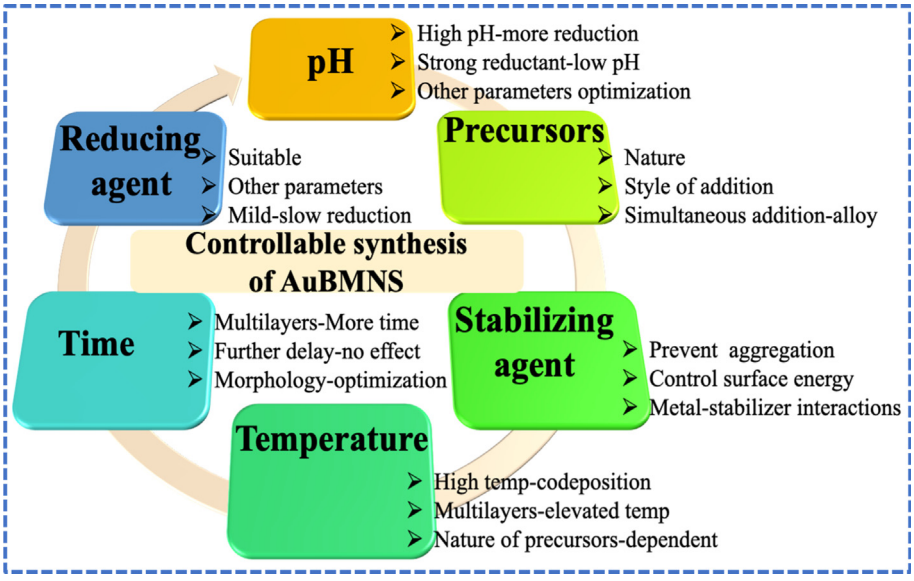

Fig. 3 Influences of important reaction parameters on the morphology-controlled preparation of AuBMNS. Shape, size, surface structure and overall morphology can be controlled by regulating the power of reductant, precursors (nature/concentration), stabilizing/coating agents, time, temperature and pH.

viously, the binding energies have been calculated by using theoretical/computational approaches like density functional theory (DFT) (Goliaei and Seriani 2019). Also, thermodynamic adjustment can be used to successfully control the surface energies and eventually obtain AuBMNS with desired morphology and structure (Nieto-Argüello et al., 2021). Inappropriately, a large number of covering/capping molecules disturb reaction parameters and produce an undesirable product (Bibi et al., 2022). This can be overcome by calculating the coverage densities through experimental and theoretical analysis (Nanda et al., 2019). Consequently, the shape and size of AuBMNS can be tuned by applying estimated surface coverage densities and optimized reaction conditions. Besides, the optimum concentrations of metal precursors and stabilizing agents can be used to obtain monodispersed and small-sized AuBMNS. Many compounds have been evaluated as reducing and capping/stabilizing agents in the formation of AuBMNS. For instance, L-cysteine was applied as a reducing as well as a stabilizing agent for the preparation of Au@Ag core–shell NPs via a one-pot synthetic approach (Siddiqui et al., 2019).

2.3. Concentration of metal precursors and style of addition

Concentration and style of addition of metal ions influence the size and shape of AuBMNS. Usually, in AuBMNS synthesis, the simultaneous addition of two metals results in the formation of alloy NPs. Though, when the reduction potential of the other metal is different, regular (layered) AuBMNS can be prepared (Liu et al., 2014, Joseph et al., 2019). For instance, the shell thickness of core–shell AuBMNS was controlled by adjusting the volume of metal precursors (Wang et al., 2021a, 2021b). The AuBMNS with shell textures of 2, 3, 5, 7, 9 and 11 nm were produced by applying different metal volumes (from 2 to 11 mL and 1 mM) (Fig. 4**).** Similarly, bimetallic hollow AuBMNS were prepared for the detection of Hg in water. The AuBMNS of different compositions were prepared by controlling the molar ratio of Ag and Au in the reaction mixture, ranging from 0.13 to 2.0. The resultant nanostructures were characterized using UV–Visible spectroscopy and transmission electron microscopy (TEM). The absorption maxima of the AuBMNS were changed from 463 to 611 nm by changing the concentration of the Au and Ag in the reaction mixture. Increase in the molar ratio (0.25–2.0) resulted in large-sized AuBMNS (from 54 to 75 nm) (Jain and Satija 2018).

In another study, a series of bovine serum albumin (BSA)-coated AuBMNS were prepared by changing the molar ratios of Au and Ag salts. Their electrochemiluminescence (ECL) property was studied by applying triethylamine (TEA) as a co-reactant. Particularly, multi-fold higher efficiency was noted for AuBMNS as compared to their monometallic counterparts (Zhai et al., 2017).

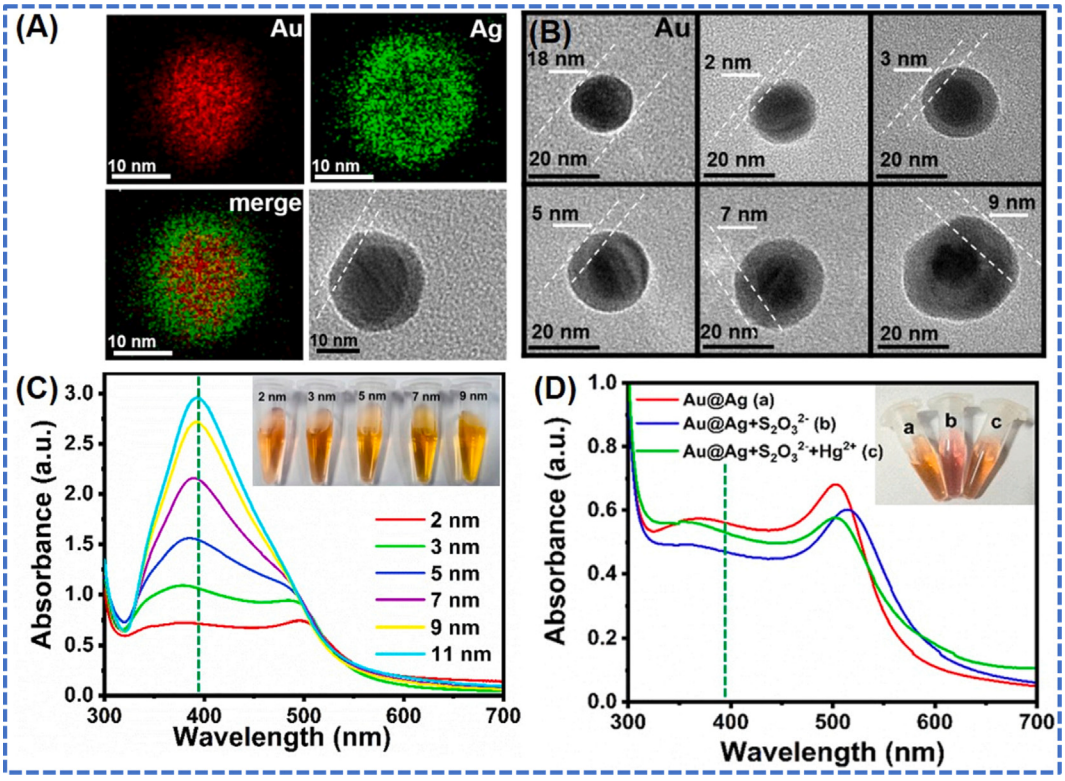

Fig. 4 **(A)** EDS mapping, **(B)** TEM images, **(C)** UV–vis absorption spectra, **(D)** Optical photographs and UV–vis absorption spectra of AuBMNS. The AuBMNS were prepared by seed-mediated method by using 20 mL of pre-formed Au NPs. The AuNPs were added into 3 mL of 0.1 M ascorbic acid at room temperature under magnetic stirring. Then, optimized volume of 1 mM $AgNO_3$ was dropwise (30 s for each drop) added into the above reaction mixture. The average size of the prepared AuBMNS was 18 nm and the shell thickness of core–shell AuBMNS was controlled by adjusting volume of metal precursors. The AuBMNS with a shell textures of 2, 3, 5, 7, 9 and 11 nm were produced by applying different metal volumes (from 2 to 11 mL and 1 mM) of metal precursor. Reprinted from Wang et al., 2021a @Copyright 2021, with permission from Elsevier.

2.4. Nature of reducing agents

For AuBMNS preparation, an appropriate reducing agent is necessary, but also, the other reaction parameters should be adjusted correspondingly. It is hard to regulate the size and shape of NPs under the influence of a strong reducing agent since it causes a fast metal ions reduction. To obtain AuBMNS with desired shape and size, weak or milder reductants can be used (Chen et al., 2019). Predominantly, reductants show a moderate/low reducing power at low pH, however their reducing power increase at high pH. Therefore, for a certain reaction, a suitable reductant should be chosen that may not disturb the nano-system. Several reducing agents such as TEA, sodium borohydride, sodium citrate, elemental hydrogen, polyols, N-N-dimethylformamide (DMF), ascorbate and Tollens reagent have been used for the preparation of Au-based monometallic and multi-metallic NPs (Ali et al., 2021a, 2021b, 2021c). For example, $NaBH_4$ was applied as a reducing agent in the preparation of Ag-Cu NPs by simply using the chemical reduction method (Kokilavani et al., 2020). In another study, BSA capped Au@Ag NPs were synthesized in an aqueous solution using a green and facile synthetic method by reacting $HAuCl_4$ and $AgNO_3$ solutions (Dai et al., 2018). Moreover, cetyltrimethylammonium bromide (CTAB) was applied as a reductant in the preparation of Au@Ag core–shell triangular nanoplates. The concentration of CTAB was found to affect the uniformity of the AuBMNS. At a higher concentration of CTAB, small-sized nanoplates were deposited in the bottom and inhomogeneous AuBMNS were obtained. However, at low concentrations, no deposition of the nanoplates was observed and uniform AuBMNS were obtained (Zhu et al., 2019).

2.5. Temperature

Temperature can speed up the co-deposition of Au atoms which results in the formation of AuBMNS. Hence, an appropriate temperature is vital for the synthesis of AuBMNS. Though, the shape and size of AuBMNS greatly depend on several other parameters such as pH, reducing/stabilizing agents, precursors concentration and time. However, the preparation of AuBMNS can be better controlled at low-temperature. Reports have shown that the preparation of bi/tri-metallic Au NPs needs a relatively higher temperature as compared to their monometallic counterparts. For example, Au-Ag core–shell triangular nanoplates stabilized with CTAB were synthesized at 65 °C under vigorous stirring (Zhu et al., 2019). Similarly, BSA-protected AuBMNS were prepared by reacting the metal precursors ($HAuCl_4$ and $AgNO_3$) at 37 °C for 12 h (Dai et al., 2018). In another report, 6 mL of ethylene glycol (EG) solution was pre-heated to 152 °C for 1 h under magnetic stirring. Then, 70 mL of Na_2S solution in EG was pipetted into this hot EG. Finally, Au@Ag hollow nanocages were obtained (Chen et al., 2020). Hence, to get thermodynamically and kinetically controlled AuBMNS, it is crucial to carry out their preparation under optimized temperature.

2.6. Reaction time

Reaction time is an important parameter for controlling the morphology of AuBMNS. It has been ascribed that extended reaction time results in a large number of NPs and promotes agglomeration of NPs. In an experiment, Au/Ag bimetallic NPs were prepared by reacting $HAuCl_4$ with pre-formed Ag NPs and the solution was stored at ambient temperature for 12 h to ensure Au atoms deposition on the surface of the Ag NPs through galvanic replacement reactions (Ismail and Dawes 2022). In another study, biopolymer capped AuBMNS were prepared by reacting the metal precursors under optimized experimental conditions in a magnetic stirrer at 70 °C (in a water bath) for 3 h (Ismail and Dawes 2022). Depending on the nature and structure of AuBMNS, the reaction time may be extended. For instance, Au@Ag core–shell nanorods were prepared by using pre-formed Au NPs. To the pre-formed Au NPs, different volumes of $AgNO_3$ (30, 50, 70, 100 and 250 μL) were added under magnetic stirring. The reaction mixture was reacted for 2 h and Au@Ag nanorods were collected by centrifugation (Chen et al., 2022). In conclusion, AuBMNS with diverse sizes and shapes can be obtained by sensibly regulating reaction conditions, and these conditions/-parameters direct the morphologies and functionalities of these nano-sensors.

3. Functionalization of AuBMNS

The stability and dispersity of AuBMNS can be associated with their ability to avoid self-aggregation or decomposition. The stability of AuBMNS can be improved by using a suitable surface functionalizing agent. The functionalization involves chemical interactions between stabilizer molecules and AuBMNS surfaces (Deng et al., 2021b). Besides, partial substitution on the AuBMNS surface through covalent coupling bonds and physical interactions can be carried out (Zhang et al., 2021). Generally, surface capping ligands containing at least a thiol group have been chemically fabricated on the surface of AuBMNS through strong Au-sulfur (Au-S) or Au-nitrogen (Au-N) bonding (He et al., 2021). The functionalization preserves the functionality, stability and unique optical characteristics of AuBMNS. The strong SPR band and light scattering property improve their behaviors toward target analytes and result in the enhancement of sensitivity and selectivity (Saeed et al., 2022).

Usually, citrate ions are not firmly bound to the surface of AuBMNS, so they can be simply substituted by using other ligands through a chemical reaction between the AuBMNS surface and suitable ligands (Chatterjee et al., 2022). Based on functionalization (Ielo et al., 2021), several biochemical molecules have been utilized to cap the AuBMNS surface Table 1. Recently, plant extracts have been applied as a sustainable and green method for the preparation of AuMBNPs with unique surface chemistry. The diverse surface chemistry of plant-extract synthesized AuBMNS have shown enhanced selectivity and sensitivity towards Hg detection (Thangaswamy et al., 2021). However, the use of different plant extracts for AuBMNS synthesis result in various surface chemistry of AuBMNS and lead to variations in the detection efficiency of the sensor (Nieto-Argüello et al., 2021, Thangaswamy et al., 2021). Hence, understanding the role of surface chemistry in Hg detection and the effect of plant extracts on the surface

chemistry of AuBMNS is crucial for the preparation of reliable and effective Hg sensors.

4. Morphology-dependent optical properties of AuBMNS

The colloidal solutions of AuBMNS display bright intense colors when interacting with light. This property is due to the free electrons which create a surface plasma state. A localized SPR is generated by these surface plasmas that resonate at a specific frequency and result in the release of energy (scattered light). The size, shape, geometry, dielectric function and nearby environment of AuBMNS determine the type of the emitted light (Kołątaj et al., 2020).

A colloidal solution of AuBMNS exhibits ruby red color. Typically, Ag NPs and Au NPs display SPR peaks in the region of 400–450 and 500–550 nm respectively (Ali et al., 2020a, Ali et al., 2020b). Similarly, SPR peaks for AuBMNS have been observed at 552 nm (Krishnan Sundarrajan and Pottail 2021). The main advantage of using AuBMNS as a colorimetric sensor is their exceptionally high molar absorptivity or molar extinction coefficient in classical UV–visible spectroscopy. This property of AuBMNS in the visible region is better than the normal organic dyes or chromophores by about 3–5 orders (Jain et al., 2020). The SPR peak varies with the morphology and structure of Au NPs. For instance, the optical nature of different Au NPs such as star-like/cubes (Alp et al., 2021), hemispherical (Liebig et al., 2018), rods (Park and Song 2021), branched/flower-like (Fu et al., 2021), prisms (Tapia-Arellano et al., 2021), octahedral (Zaheer 2021) NPs have been described. Reports have shown that by increasing the size of the NPs, redshift occurs in the SPR, as well as the accumulation of NPs results in a shift in the SPR band (Dung et al., 2021). Optical analysis has exposed that granule-like NPs display low transmittance and high absorption, while plate-like NPs show high transmittance (Amirjani and Haghshenas 2018). For spherical NPs, the electric field of the metal surface is the total field generated by the electric field and SPR, which can be calculated by using the below equation (Kołątaj et al., 2020, Wang et al., 2020).

$$\left| E_{out} = E_0 \overrightarrow{x} - \alpha E_0 \left[\frac{\overrightarrow{x}}{r^3} - \frac{3x}{r^5} \left(x\overrightarrow{x} + y\overrightarrow{y} = z\overrightarrow{z} \right) \right] \right.$$

In this equation, α is the metal polarizability, x, y, z are Cartesian coordinates, →x, →y, →z are unit vectors and r is the radial distance.

According to Mie's theory, the extinction cross-section (Cex) of spherical NPs can be computed by applying the below equation (Rycenga et al., 2011).

$$\left| C_{ext} = \frac{24\pi^2 R^3 \varepsilon_m^{3/2}}{\lambda} \left[\frac{\varepsilon_i}{(\varepsilon_r + 2\varepsilon_m)^2 + \varepsilon_i^2} \right] \right.$$

In this equation, the radius of the spherical NPs is represented by R and the refractive index of the medium is denoted by εm.

Theoretical studies have exposed that for larger NPs a quadrupole mode could be excited while only dipole modes could be excited for smaller NPs when irradiated with light (Kołątaj et al., 2020). Besides, the distribution of electric fields around the NPs changes with the transformation of NPs shape. For example, Ag nano-rods show double plasmon peaks, with excitation along the long axis and short axis. For triangular nano-prisms, four plasmon peaks can be observed; out-of-plane quadrupole, in-plane dipole, weak out-of-plane dipole and in-plane quadrupole (Boken et al., 2017).

The sensing efficiency and SPR of AuBMNS depend on many variables including shape, size, composition, morphology, inter-particle distances, orientation, dielectric constant of the surrounding medium and surface chemistry of NPs. However, size and shape are vital features (Kaviya 2020). Hence, AuNPs have been extensively applied for heavy metal ions sensing by taking benefit of their diverse morphologies (Yu et al., 2020). The changes in SPR bands when the size/shape of the NPs are because different NPs have different extinction spectra in the ultraviolet–visible region (He et al., 2020). Hence, the NPs show characteristics SPR bands dependent on their shape and size, state of aggregation and external environment. This offer an outstanding platform for proposing Au NPs-based sensors for chemical and biological fields (Yao and Santos 2020). Comparatively, the SPR of non-spherical NPs has a more spectral shift than that of spherical Au NPs owing to the relatively strong electric fields on the surface with high curves (Yu et al., 2020). UV–vis spectroscopic analysis has been applied to establish the molar extinction coefficient of AuBMNS with different capping ligand monolayers and different sizes (Chen et al., 2021). Based on the morphological-dependent optical properties of AuBMNS, they have been applied in colorimetric, fluorescence, electrochemical, combined techniques and SERS detection of Hg (Fig. 5). Moreover, in the latest literature survey, the core–shell AuBMNS composed of Ag and Au atoms have been widely used as nano-sensors for Hg detection (Table 1).

5. Role of surface chemistry and morphology of AuBMNS in Hg detection

AuBMNS have shown promising application in Hg detection due to their distinctive surface chemistry and morphologies. The surface chemistry of AuBMNS can be definitely adjusted to enhance their selectivity and sensitivity towards Hg. This can be accomplished through the functionalization of their surfaces with different ligands (Chatterjee et al., 2022). The morphology of AuBMNS also plays a vital role in Hg detection as their large number of surface-active sites and high surface area to volume ratio allow for efficient detection of Hg ions (Joseph et al., 2019). Moreover, the bimetallic nature of AuBMNS enables their synergistic effect and leading to enhanced sensing properties (Fernandes et al., 2021). Significantly, the combination of morphologies and surface chemistry AuBMNS provides a promising platform for the development of highly selective and sensitive sensors for Hg detection (Becerril-Castro et al., 2022, Chen et al., 2020).

The use of plant extracts for AuBMNS synthesis is beneficial over other methods as it is cost-effective and eco-friendly. However, plant extracts synthesized AuBMNS have an extremely complicated surface chemistry, which varies from plant extract to plant extract (Ali et al., 2020c, Ali et al., 2021a, 2021b, 2021c). AuBMNS synthesized using plant extracts show a distinctive surface chemistry that can be adjusted for specific applications. Owing to the specific surface chemistry of AuBMNS, they can bind selectively to Hg ions, leading to enhanced detection sensitivity. Hence, the synthesis of

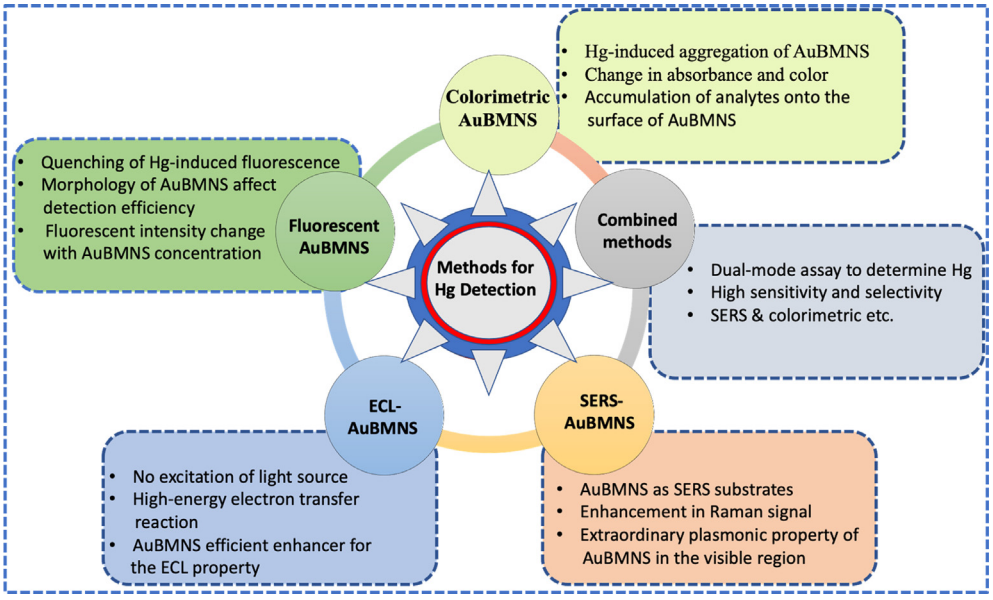

Fig. 5 Overview of the frequently applied detection methods for AuBMNS-based Hg detection. AuBMNS have been applied in colorimetric, fluorescence, electrochemical and SERS detection of Hg. These methods can be applied in combination to improve the sensitivity and selectivity towards Hg detection.

AuBMNS using plant extracts holds great potential for the development of sensitive and efficient detection systems for Hg ions (Thangaswamy et al., 2021).

Studies have shown that the detection efficiency of AuBMNS depends on their nature, surface ligands, composition and morphology **(**Table 2**)**. For instance, nafion stabilized l-cysteine-capped Au@Ag core–shell AuBMNS of size 43 nm were applied for Hg^{2+} detection in different groundwater samples, and the limit of detection (LOD) was about 0.5 nM (Siddiqui et al., 2019). Zeolitic imidazolate framework-8 derived Ag@Au core–shell AuBMNS of size 20 nm were used for Hg^{2+} detection in water samples and LOD of 1.8 ± 0.04 nM was achieved (Salandari-Jolge et al., 2021). Moreover, Apt-Cu@AuAuBNPs were applied for Hg^{2+} determination in Porphyra up to 4.92 nM (Shi et al., 2021) (Fig. 6 **(A)).**

The detection efficiency of NPs towards Hg ions also depends on their nature. Often, bimetallic NPs are more sensitive and selective towards Hg ions detection. For instance, monometallic and bimetallic NPs of Au and Ag were synthesized via the green method using an aqueous extract of *Chlorella acidophile* and examined for Hg detection. The bimetallic NPs were found more efficient in the detection of Hg as compared to their monometallic counterparts (Thangaswamy et al., 2021).

The composition of AuBMNS influences their performance. For example, spherical Au@FeAuBMNS were applied to detect Hg in a real water sample by using a colorimetric method, and LOD of 1.0 nM was achieved (Liu et al., 2022b). On the other hand, the same spherical Au@Ag AuBMNS with different compositions were used for Hg detection in water and 5 nM LOD was obtained (Zhai et al., 2017). This show that the compositions of AuBMNS have a strong correlation with their detection efficiency.

In a study, Hg was detected in water up to 5 nM by using spherical BSA-protected Au@Ag NPs of size 2.3 nm (Zhai et al., 2017), while chitosan modified rod shape Au@Ag NPs of size 16 nm and pointed tips shape Au@Ag NPs (AA and CTAB functionalized) exhibited LODs of 0.9 nM and 5 nM respectively for the determination of the same analyte (Zhang et al., 2019). These studies show that the detection of Hg ions was greatly affected by the size and shape of the AuBMNS **(**Tables 1 and 2**)**.

The detecting efficiency of AuBMNS was found to be greatly affected by the functionalizing/stabilizing agents used in the NPs formation. For instance, Hg was detected up to 4.8 nM by lysine-caped spherical Ag@Au NPs of size 55 nm (Bi et al., 2021), while BSA functionalized Ag@Au NPs of size 3 nm and Tetraoctylammonium bromide (ToABr) modified Ag@Au NPs detected the same analyte (Hg) up to 0.35 nM and $1.5x10^{-7}$ M respectively (Pawar et al., 2019, Liu et al., 2020). Furthermore, Hg^{+2} was detected in water (up to 0.88 nM) by using CTAB modified Ag@Au NPs (core–shell triangular nanoplates) of size 122 nm (Zhu et al., 2019). On the other, the same analyte (Hg^{+2}), in the same medium (water), was detected up to 10 nM by using DNA aptamer-modified AuBMNS of size 120 (Lu et al., 2018). These examples demonstrate that the sensing of the same ion (Hg^{+2}) was strongly affected by the nature of the stabilizing/functionalizing agent of the AuBMNS.

Recently, various AuBMNS have been applied for Hg^{+2} detection. For example, zeolitic imidazolate framework modified cubic Ag@Au NPs of size 20 nm exhibited LOD up to 0.018 nM (Salandari-Jolge et al., 2021), while spherical Ag@Au NPs of size 18 nm detected the same ion up to 200 nM (Wang et al., 2021a, 2021b) and Au@Ag core/shell NPs of size 43 nm detected the ion up to about 0.5 nM (Siddiqui et al., 2019). Hence, a strong association between the LOD and size/shape/capping agents of BMNNPs can be observed while using these NPs for

Table 2 Comparison, detection method and nature of different AuBMNS-based sensors for Hg determination.

S. No.	Type of AuBMNS	Sample	LOD	Detection mechanism	Ref.
1	Au@Fe	Real water	1.0 nM	Colorimetric	(Liu et al., 2022a, 2022b)
2	Au@Ag core–shell	River water	0.9 nM	Naked-eye detection	(Zhang et al., 2019)
3	BSA-protectedAg@U NPs	Water	5 nM	ECL	(Zhai et al., 2017)
4	Lysine-capedAg@Au NPs	Aqueous solutions	4.8 nM	tion	(Bi et al., 2021)
5	Ag@Au NPS	Pool water	5 nM	Selective etching/colorimetric	(Xing et al., 2018)
6	Ag@Au Nanoclusters	Aqueous solutions	0.35 nM	Fluorescence	(Liu et al., 2020)
7	Ag@Au Alloy NPs	Water	1.5×10^{-7} M	SERS	(Pawar et al., 2019)
8	Au@AgHollow nanocages	Lake and tap water	10 nM	Etchinginduced morphology transformation	(Chen et al., 2020)
9	Ag@AuNanocluster	Fish and rice samples	10 μg L^{-1}	Ratiometric and visual detection	(Dai et al., 2018)
10	Au@SiO_2Core-shell NPs	Tap water	1.25 ng/mL	Fluorescence	(Zhu et al., 2018)
11	Au-Ag core–shell triangular nanoplates	Lake water	0.88	etching-induced spectrum change	(Zhu et al., 2019)
12	Au@SiO_2 core–shell NPs	Water	10 nM	SERS	(Lu et al., 2018)
13	AuNCs-Ag@Keratin	Real water	2.31 nM	Fluorescence quenching mechanism	(Wang et al., 2018)
14	Au@S-C_3N_4	River water samples	0.275 nM	Colorimetric	(Amanulla et al., 2019)
15	Fe_3O_4@Au Core-shell NPs	Water and fish samples	0.5 μg L^{-1}	Electrochemical	(Butmee et al., 2021)
16	Au-Pt@C Nanofiber	Real water samples	3.33×10^{-16} mol/L	Electrochemical	(Xie et al., 2021)
17	Ag@AuHollow nanostructures	Real water	10 pM	Colorimetric	(Jain et al., 2020)
18	Ag@Au NPs	Real water	0.526 mg L^{-1}	Colorimetric	(Mathaweesansurn et al., 2020)
19	Ag-coated AuNPs	Real water	78 nM	Colorimetric and visual detection	(Da et al., 2018)
20	A@C_3N_4 Nanocomposites	Real water	3.0 nM	colorimetric	(Wang et al., 2019)
21	Ag@AuCore-shell NPs	Groundwater sample	0.1 ppt	Voltametric	(Siddiqui et al., 2019)
22	Au@Pd NPs	Actual water sample	0.16 nmol/L	Electrochemical	(Wang et al., 2022a, 2022b, 2022c, 2022d, 2022e)
23	Au@Cu nanoclusters	Porphyria	4.92 nM	Ratio-metric fluorescent	(Shi et al., 2021)
24	Ag@Au NPs	River, tap and wastewater samples	1.8×10^{-17} M	Electrochemical	(Salandari-Jolge et al., 2021)
25	Au@Ag NPs	Real water and Chinese medicines	0.2 μM	Colorimetric and SERS dual-mode	(Wang et al., 2021a, 2021b)

Hg^{+2} detection (Guo et al., 2021, Jadoun et al., 2021, Mitchell et al., 2021).

6. Mercury detection using AuBMNS via various methods

6.1. Colorimetric AuBMNS for Hg detection

AuBMNS-based colorimetric sensors have been widely reported for their sensitive and selective detection of Hg (Chansuvarn et al., 2015, Gul et al., 2022). This is due to their very high molar absorptivity or extinction coefficient, ε (M^{-1} cm^{-1}). The ε of Au based NPs is higher in the visible region as compared to conventional organic dyes or chromophores by about 3–5 orders (Rosi and Mirkin 2005).

In a study, SDS capped spherical Ag@Au hollow nanostructures of size 26 nm were synthesized via a reduction/heteroepitaxial seed-mediated approach and applied for colorimetric detection of Hg in a real water sample. The comparative evaluation of the developed Ag@Au hollow nanostructures revealed relatively high sensitivity toward Hg detection as compared to their monometallic counterpart, and the LOD was 10 pM (Xie et al., 2021).

In another study, agar-stabilized core–shell Ag-coated AuNPs of size 19 nm were prepared via a two-step reduction method and applied for Hg detection in real water up to 78 nM. The sensing of Hg was based on the suppression of the interaction of agar-stabilized Au@Ag NPs with dithiothreitol (DTT). The method presents the benefits of portable feasibility, visual detection and easy operation (Da et al., 2018). In addition, the colorimetric method can be combined with other techniques to improve the Hg detection efficiency. For instance, a colorimetric method was employed in combination with the SERS technique and Hg was detected up to 0.2 μM in Chinese medicines and real water samples (Wang et al., 2021a, 2021b).

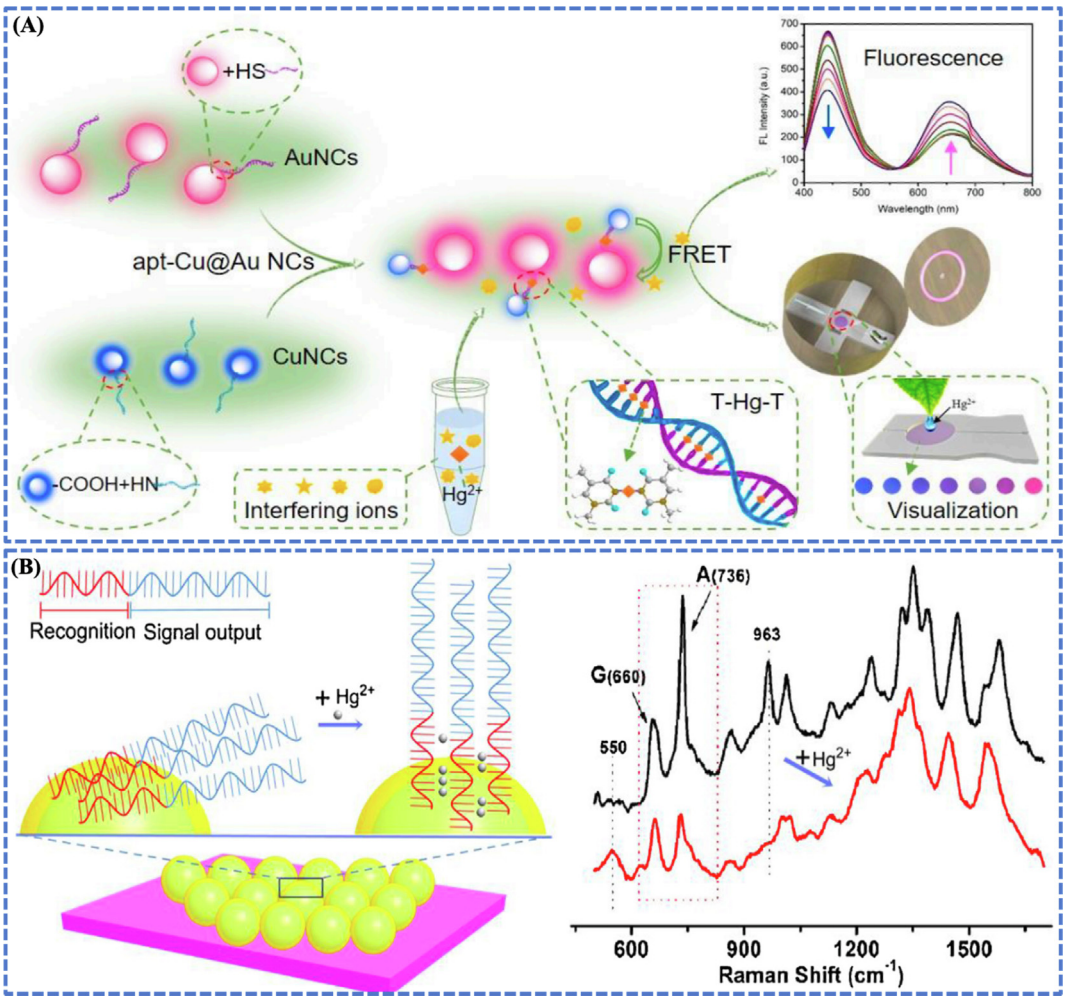

Fig. 6 **(A)** Aptamer-modified AuBMNS based ratio-metric fluorescent probe for Hg^{2+} detection in Porphyra. The NPs were uniformly-dispersed in solution in the absence of Hg^{2+}, while accumulated together due to the formation of thymidine-Hg-thymidine (T-Hg-T) structure upon the addition of Hg^{2+}. This resulted in the changes (visible to naked eye) in their fluorescence signals due to FRET. Finally, Hg^{2+} were detected ranging from 0.1 to 9.0 μM by the proposed fluorescence system with the LOD of 4.92 nM. Reprinted from Shi et al., 2021 @Copyright 2021, with permission from Elsevier. **(B)** The label-free SERS sensor was based on the formation of T-Hg-T bonds and the consequent alignment of DNA on the surface of Au shell. The consecutive T acted as the Hg^{2+} identification elements, and the segment with guanine and adenine (G and A) bases served as the signal reporters. When Hg^{2+} interacted with the T, it resulted in the enhancement of Raman intensity and allowed to measure low level of Hg^{2+} in aqueous solution. Based on the label-free SERS sensor, Hg^{2+} was determined within a wide concentration range from 1×10^{-8} to 1×10^{-3} M. Reprinted from Lu et al., 2018 @Copyright 2018, with permission from Elsevier.

Hg-induced aggregation of AuBMNS is the main detection mechanism, leading to a change in absorbance and color (Ali et al., 2021a, 2021b, 2021c). The changes in absorbance and color of colloidal AuBMNS through Hg-induced disassembly and accumulation of analytes onto the surface of AuBMNS have been applied in the detection of Hg ions in different samples (Bi et al., 2021). Additionally, the selectivity and sensitivity of AuBMNS depend on several parameters, such as concentration of AuNPs, particle size, the concentration of Hg in a sample, pH, temperature, ionic strength, and composition of the surrounding solution (Yu et al., 2021). Previously, colorimetric analyses based on AuBMNS have been extensively reported in various research areas. These methods include but are not limited to colorimetric detection based on the aggregation of functionalized AuBMNS, colorimetric approaches based on the aggregation of un-functionalized AuBMNS, detection based on removal of protecting ligand from the surface of AuBMNS and detection based on non-aggregation of AuBMNS induced by appropriate ligands (Chansuvarn et al., 2015).

6.2. Fluorescent AuBMNS for Hg detection

Irregular-shaped AuNCs-Ag@Keratin of size 2.63 nm were prepared by using the chemical reduction method, the materials were modified with Ag(I) ion and applied for Hg detection in real water. Based on the fluorescence quenching mechanism, a LOD of 2.31 nM was achieved (Wang et al., 2018).

In another study, amino-modified core–shell $Au@SiO_2$ NPs were prepared by using pre-formed AuNPs and SiO_2,

applied for Hg detection in tap water and LOD of 1.25 ng/mL was obtained (Zhu et al., 2018). Similarly, BSA functionalized spherical Ag@Au nanoclusters of size 3 nm synthesized via chemical reduction were used to detect Hg in aqueous solutions by using a fluorescence mechanism and LOD of 0.35 nM was obtained (Liu et al., 2020), as shown in Fig. 7**A.**

The fluorescence detection principle of AuBMNS is based on the quenching of Hg-induced fluorescence. Generally, the fluorescent intensity of AuBMNS decreases upon increasing the concentration of Hg^{2+}. A linear plot of fluorescence ratios at a specific wavelength versus log [Hg] or a plot of comparative fluorescence of AuBMNS as a function of [Hg] is applied as a calibration curve (Zhang and Guo 2022). Likewise, AuBMNS need no additional protecting or stabilizing molecules to prevent their self-aggregation. Several studies have been reported to prepare fluorescence active AuBMNS and applied them for Hg detection (Chatterjee et al., 2022).

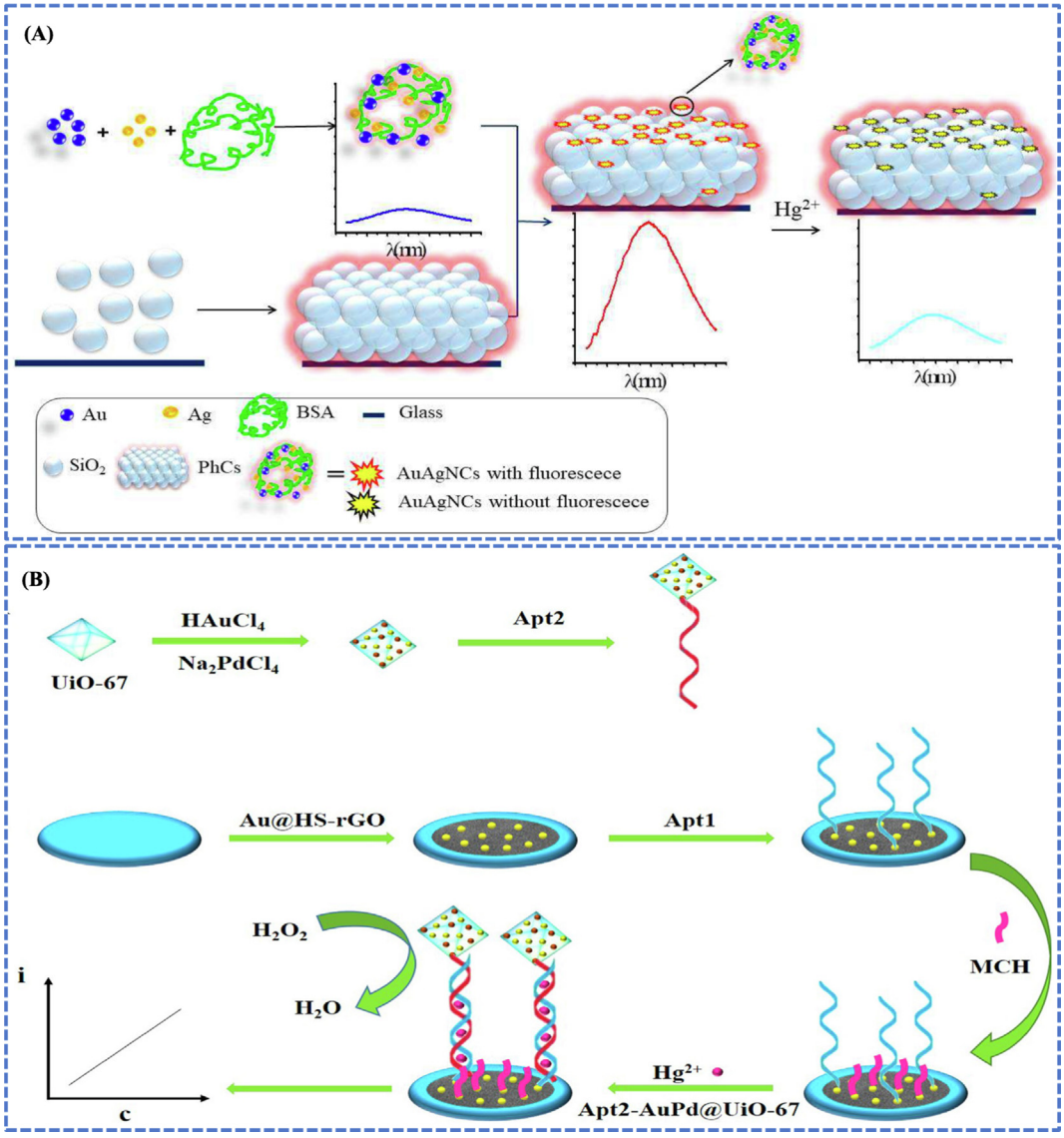

Fig. 7 **(A)** Hg detection based on fluorescent AuBMNS. BSA functionalized spherical Ag@Au nanoclusters of size 3 nm synthesized via chemical reduction were used to detect Hg in aqueous solutions by using fluorescence mechanism. The fluorescence intensity of the AuBMNS was enhanced up to 8.0-fold by PhCs relative to the control sample (no PhCs) and LOD of 0.35 nM was obtained. Reprinted from Liu et al., 2020 @Copyright 2020, with permission from Elsevier. **(B)** AuPd@UiO-67 were used as signal enhancer for sensing Hg^{2+}. Au NPs were fabricated on HS-rGO to obtain a thin layer of Au@HS-rGO. The Apt1, as substrate strand, was modified on the system via Au-S bond. The Apt2, as signal strand, was fabricated on the sensing system in the presence of Hg^{2+}. The Apt2 was modified with AuPd@UiO-67 nano-zyme, which showed catalase-like activities to catalyze H_2O_2 and produced electrical signal. When Hg^{2+} concentration was increased, the amount of fabricated Apt2-AuPd@UiO-67 increased and resulted in the enhancement of current response. The concentration of Hg^{2+} was found linear with current responses. The organized electrochemical apta-sensor showed a wide linear range (1.0 nmol/L to 1.0 mmol/L) along with LOD of 0.16 nmol/L. Reprinted from Wang et al., 2022a, 2022b, 2022c, 2022d, 2022e @Copyright 2022, with permission from Elsevier.

6.3. SERS-AuBMNS for Hg detection

The AuBMNP-based SERS sensors have great potential for the real-time detection and monitoring of Hg in biomedical and environmental applications. Several studies have been reported in the literature on the influence of size, shape and composition of mono-metallic and multi-metallic NPs in SERS efficiency, because plasmonic properties of NPs depend upon their anisotropy, shape, size and intrinsic dielectric functions (Becerril-Castro et al., 2022). For instance, Gao et. al. have described that fully alloyed Ag@Au nanospheres showed better plasmonic properties as compared to the individual Au or Ag nanospheres owing to the synergist combination of the plasmonic activity of Au and Ag (Si et al., 2018). Shweta Pawar et al have observed 30 times improvement with Ag@Au (90:10) micro-flower as compared to the pure Ag micro-flower (Pawar et al., 2019). They assumed that the enhancement was due to the surface-rich Ag in the alloy. Yilin Lu et al have detected Hg up to 10 nM in water by using DNA aptamer-modified Au@SiO_2 spherical core/shell NPs of size 120 nm (Lu et al., 2018), as shown in Fig. 6 **B**. The DNA aptamer immobilized on the surface of the NPs was comprised of consecutive thymine (T) bases, acting as the Hg^{+2} sensing elements, and the adenine (A) and guanine (G) bases was serving as the signal reporters. When Hg^{2+} ions interacted with the thymine, the DNA molecule assumed vertical alignment, resulted in the enhancement of Raman intensity ratio I (660 cm^{-1})/I(736 cm^{-1}) with an increase in Hg^{2+} concentration. Hence, it was made possible to measure a very low level of Hg^{2+} in water quantitatively and selectively. Similarly, *Sujin* et al have prepared spherical Ag@Au NPs of size 5–45 nm by employing the green method (from the extract of *Chlorella acidophile*). A more pronounced and enhanced Raman spectra of the Au@Ag NPs compared to their monometallic counterparts were observed and the materials were recommended for sensing applications in industries (Thangaswamy et al., 2021).

The mechanism of Hg detection based on AuBMNS and SERS involves the interaction of Au and Hg on the NPs surface, which leads to a change in the Raman scattering frequency and intensity of the adsorbed molecules. The presence of Hg results in a red-shift in the Raman peak, which can be applied as a selective and sensitive indicator of Hg detection (Pawar et al., 2019). Moreover, Ag@Au NPs are the best choice owing to their extraordinary plasmonic property in the visible region (Zhang et al., 2019). Recently, promising studies regarding AuBMNS-SERS detection of Hg have been reported (Tim et al., 2021). Interestingly, spectra with significant enhancement factors have been described by applying AuBMNS of different morphologies (Lu et al., 2018, Pawar et al., 2019). The combination of SERS and AuBMNS offers a highly specific and sensitive method for Hg detection in complex samples.

6.4. ECL AuBMNS for Hg detection

ECL has been extensively used in environmental monitoring and immunochemical assays (Ma et al., 2021). ECL emission is produced from electrochemical high-energy electron transfer reactions rather than the excitation of a light source. Hence, it prevents the scattering of light and also has other advantages, such as easy operation, high sensitivity and lower background signal (Gu et al., 2021). The first ECL emitter of silica NPs was described in 2002, such as carbon nanodots and semiconductor nanocrystals (Ge et al., 2021). Recently, metal nanomaterials with special electronic, optical and chemical behaviors have gained significant attention in ECL detection owing to their low toxicity and molecule-like properties (Zhang and Wang 2014). Interestingly, Au-based NPs with enhanced catalytic activity, excellent stability, ease of synthesis and good water solubility have attracted extensive interest in ECL from the analytical to fundamental field (Kukreti and Kaushik 2021). Recently, AuBMNS have attracted particular interest in ECL as compared to monometallic NPs, because they share synergistic properties of two elements and display more superior efficiencies in optical, catalytic and electronic aspects (Nikolaou et al., 2021). Qingfeng Zhai et al have prepared spherical BSA-protected Ag@Au NPs of size 2.3 nm, and reported their sensing efficiency for Hg detection in water and LOD of 5 nM was achieved (Zhai et al., 2017). Furthermore, they investigated the ECL property of the Au@AgNPs using different molar ratios of metals (Au and Ag) and TEA as a co-reactant. The doping of Ag into Au NPs resulted in a higher ECL emission; this is due to the synergistic effect of the two atoms. The ECL was enhanced up to 5 times for the bimetallic NPs as compared to their monometallic counterparts. The Ag atom was found to be served as an efficient enhancer for the ECL property. Aptamer modified Au-Pt@C nanofibers of size 400 nm were prepared by hydrothermal method and electrodeposition and applied for Hg detection in real water samples up to 3.33×10^{-16} mol/L. The Au-Pt@C sensor took the benefit of synergistic effects to enhance the electrical signal, which was applied to detect Hg with high sensitivity and selectivity (Xie et al., 2021). Irregular spherical shape Au@Pd NPs of size 110 nm were applied to electrochemically detect Hg in actual water samples and 0.16 nM/L LOD was reported (Wang et al., 2022a, 2022b, 2022c, 2022d, 2022e), as depicted in Fig. 7**B**. These reports showed that the electrochemical detection of Hg^{+2} in food and environmental samples has been proven to be an effective and sensitive method.

The recommended mechanism of Hg detection based on ECL AuBMNS involves the application of AuBMNS for effective binding of Hg ions. The AuBMNS act as a catalyst for the electrochemical reaction, resulting in the generation of reactive oxygen species and the production of ECL. The ECL signal can then be detected and measured as a marker of the amount of Hg ions in the sample (Zhai et al., 2017).

6.5. Combined methods for Hg detection

To improve the sensitivity, selectivity and applicability of AuBMNS-based sensors, two or more detection methods can be employed. For instance, spherical Au@Ag NPs (of size 18 nm) were prepared by seed-mediated reduction method and applied as colorimetric and SERS dual-mode sensors for Hg^{+2} detection in real water and Chinese medicines. The dual-mode (SERS and colorimetric) action and controllable etching of Au@Ag NPs were used and LOD of 0.2 μM was obtained (Wang et al., 2021a, 2021b), as described in Fig. 8**A**.

Irregular-shaped (5 nm) BSA stabilized Au@Ag NPs were prepared by a one-step green method and applied for Hg^{+2}

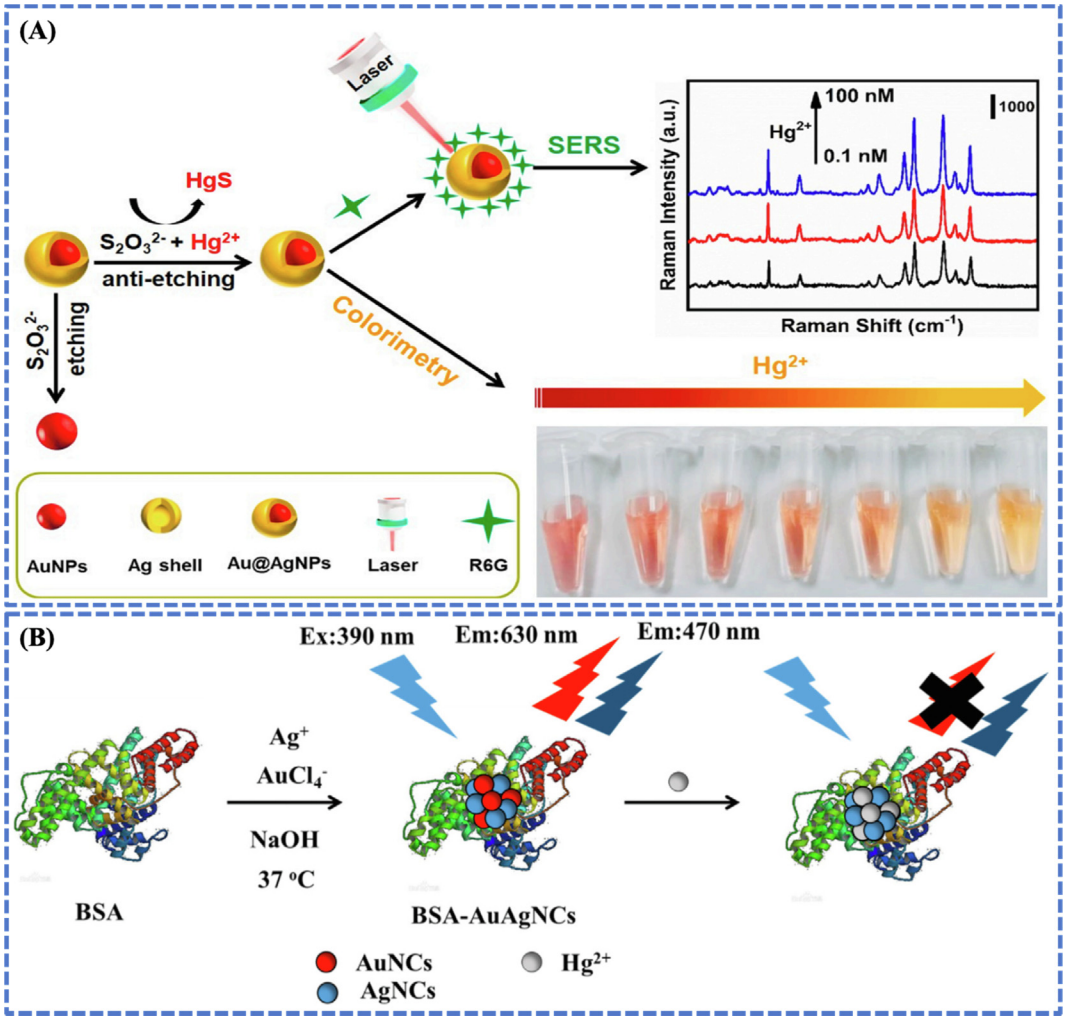

Fig. 8 **(A)** Spherical Au@Ag NPs (of size 18 nm) were prepared by seed mediated reduction method and applied as colorimetric and SERS dual-mode sensor for Hg detection in real water and Chinese medicines. The Raman intensity and UV–vis absorption increased when the silver shell was etched by $S_2O_3^{2-}$. The LOD was 0.2 μM and 2 μM through the UV–vis spectroscopy and naked eye, respectively. The LOD of SERS technique was 0.1 nM with a linear regression for the concentration of Hg^{2+} (0.1 nM^{-1} μM). Reprinted from Wang et al., 2021b @Copyright 2021, with permission from Elsevier. **(B)** Irregular shaped (5 nm) BSA stabilized Au@Ag NPs were prepared by one step green method and applied for the detection of Hg in fish and rice samples. The fluorescence of the Au@Ag NPs was rapidly and significantly quenched by interacting with Hg. When Hg was introduced into the sensing system, an obvious fluorescence quenching was observed and fluorescence color changed from red to pale blue. The observed quenching phenomenon was attributed to the formation of Hg-Au bond. A relative standard deviation (RSD, n = 7) of 0.7% at 50 μg L^{-1} Hg^{2+} concentration was achieved by applying a commercial fluorescence spectrophotometer and LOD of 2.2 μg L^{-1} was obtained. In visual sensing, Hg^{2+} was detected up to 10 μg L^{-1} from the blank with naked eye. Reprinted from Dai et al., 2018 @Copyright 2018, with permission from Elsevier.

detection in fish and rice samples (Fig. 8 **B**). The BSA stabilized Au@Ag-based sensor was applied for a ratio-metric fluorescent sensor for highly sensitive and selective detection of Hg^{+2} and LOD of 10 μg L^{-1} was obtained. The fluorescence of the Au@Ag NPs was rapidly and significantly quenched by interacting with Hg^{+2}. When Hg^{+2} was added to the system, the Au@Ag NPs solution showed an obvious fluorescence quenching phenomenon and the fluorescence color turned from red to pale blue (Dai et al., 2018).

7. Key challenges and prospects

7.1. Controllable synthesis and development of AuBMNS-sensors

AuBMNS can be prepared under an optimized state, however, when there is an alteration in experimental conditions, their morphology, shape and size change accordingly. Because changing in any experimental parameter may affect the preparation procedure and result in uncertainty in reaction conditions (Huang et al., 2021b, Zhu et al., 2022). Though, the chemical reduction approach is considered an easily control-

lable and effective way of AuBMNS preparation, it still experiences some difficulties at the atomic level. Hence, understanding the molecular/atomic level reduction mechanism will eventually allow researchers to overcome the limitations more attractively. Core-shell AuBMNS are often concerned with limitations such as non-uniformity, rough surfaces, polycrystallinity, poorly-distinct composition and difficulty to substitute the templates without disturbing the shells. Similarly, the preparation of ultra-fine AuBMNS is still a persistent challenge.

Problems are still existing in the preparation of monodisperse and uniform nano-size AuBMNS, and it is difficult to tune the shape and structure of AuBMNS (Quyen et al., 2014). Besides, unlike monometallic NPs, the actual structure, size distribution and topographical features of AuBMNS can be hardly retained while further modifying their surface features (Liu et al., 2009). Hence, it is better to combine the modification and preparation of AuBMNS in a simultaneous single step, and to improve the prevailing in-situ preparation methods of AuBMNS with appropriate substrate templates (Emam et al., 2017). Generally, researchers observe and confirm the preparation/characterization data of AuBMNS and credit the influence of parameter(s) in the preparation of AuBMNS. However, the exact design of AuBMNS for preferred purposes needs further exploration. Likewise, the morphology-controlled preparation of Au and Ag-based AuBMNS has been explored in several reports, while the other multi-metallic nano-systems still need further study. Fascinatingly, the surface structures of AuBMNS regulate their probable performance, consequently, a thorough study of their stable structures is of significant importance, and this will offer ultimate insights into the functionality, structural features, and optical behavior of AuBMNS (Fan et al., 2016, Liu et al., 2016). The capping/stabilizing agents (existing and new) can direct the morphology development of AuBMNS and these systems should be manipulated by using the molecular-level understanding of the interactions between the functional groups of stabilizing/capping agents and the surface facet of AuBMNS. Moreover, the cost of Au is very high, which is not appropriate for the informal application. Thus, another goal is to reduce the cost, this can be done by designing ultra-thin structures and/or replacing the Au with inexpensive metals.

7.2. Standardization and performance comparison of AuBMNS-sensors

Despite the significant progress made in AuBMNS, challenges persist in the development of more reliable and practical sensors to overcome critical detection issues. The sensing efficacy of AuBMNS towards Hg remains ambiguous at the molecular/atomic level and needs further clarification. For example, in core–shell NPs, it is unclear how the core elements control the surface behavior of AuBMNS, how preparation methods affect the reactivity of functional groups towards Hg, and how biocompatibility and stability can be upgraded by incorporating other elements. Moreover, several challenges remain to be resolved for the in-field practical application of AuBMNS, including long-term biosafety, easy preparation, quality control, large-scale production, and our limited knowledge of their preparation/interaction mechanisms. Hence, sophisticated theoretical analyses and mathematical studies (e.g., DFT) are essential to explore the AuBMNS preparation mechanism and interactions with Hg (McLamore et al., 2017). As reviewed in this article, AuBMNS have been extensively applied in Hg detection. However, there are comparatively fewer reports in the literature related to the practical and hand-held applicability of AuBMNS-sensors. Likewise, Au-based tri-metallic NPs are relatively unexplored as compared to AuBMNS, while their sensing performance towards Hg is expected to be more efficient than the AuBMNS (Elayappan et al., 2020, Bai et al., 2022). So, skillful designing of Au multi-metallic NPs with appropriate shape/size and compositions may result in highly effective sensors for Hg detection. We propose that an organized framework is to be formulated for Hg detection in environmental and food samples and next-generation advanced nano-sensing.

Like organo-Hg species and inorganic Hg, Hg^0 is toxic, even in low concentrations (ppb), and detection/removal of trace amounts of Hg^0 from any media is a challenging task. In the literature survey, fewer studies have been noticed on the detection and elimination of Hg^0 as compared to Hg^{2+} species. To cope with this serious challenge, the research community should develop efficient, cost-effective and portable AuBMNS-based sensors for the trace detection of Hg^0 species in food matrices and environmental samples. Interestingly, changing the configurations, morphology and composition AuBMNS can provide smart tools for sensitive and selective detection of Hg^0/Hg^{+2}. These developments in AuBMNS will be predictable to offer a stable and solid manifesto for the sensing of Hg as well as other toxins. Buoyantly, the evolving synthetic approaches of AuBMNS and technological developments in sensing strategies will fill the void.

8. Conclusion and future trends

Several methods are working to monitor and control Hg contamination in environmental samples and food matrices. One such approach is the use of noble metals NPs-based sensors for Hg detection. Among the NPs-based sensors, Au NPs have the unique advantage of low toxicity, easy method of preparation and tunable surface morphology, and have been extensively applied in Hg detection. Reports have shown that Au bimetallic NPs exhibited high sensitivity and selectivity as compared to their monometallic counterparts due to the synergistic action of the two atoms present in the AuBMNS. Moreover, the shape and size of the AuBMNS have a strong influence on their sensing efficiency. However, there is no facile way to control the size, shape and morphology of AuBMNS. Significantly, the precise optimization of reaction parameters could be applied to attain the anticipated AuBMNS. Different morphologies of AuBMNS have been prepared via optimizing reaction parameters such as pH, temperature, reducing agents, time, concentration/nature of precursors and stabilizing/capping agents, etc. Moreover, different colorimetric, SERS, fluorescence, electrochemical and combined methods have been applied for sensitive and selective detection of Hg in environmental samples and food matrices.

Beside these accomplishments, several important contests still exist. Chemically, new schemes on surface make-up control of AuBMNS at the atomic level are vital. Generally, the current approaches are empirical/semiempirical, and for most

AuBMNS preparation procedures, the principal chemistry needs to be further investigated. Unfortunately, very few AuBMNS have been recommended for practical in-field application as compared to a huge number of reports in peer-reviewed journals. Consequently, it is crucial to design applicable and innovative AuBMNS that could be practically applied in Hg detection in environmental and food samples. Also, with the help of computational practices and multi-field approaches, the down-to-earth application of the AuBMNS can be extended to hand-held sensors. Moreover, efforts are needed to fabricate and design plasmonic AuBMNS to achieve efficient coupling of plasmon with SERS or/and fluorescence to amplify signals. This will facilitate the commercialization of the coupled (plasmonic, SERS and fluorescence) probes. The commercial availability of these sensing probes will boost the application of AuBMNS-sensors in different fields. Hence, the forthcoming research should be focused on practically designing/validating AuBMNS-based sensors for their novel features and successive application in the area where they have not yet been explored. Undeniably, the upcoming era looks vivid for the morphology-controlled synthesis and application of AuBMNS.

Funding

This work has been financially supported by the Wenzhou University China scientific research start-up fund (QD2021155). The researchers would like to acknowledge deanship of scientific research, Taif University for the funding of this work.

Declaration of Competing Interest

The authors declare that they have no known competing financial interests or personal relationships that could have appeared to influence the work reported in this paper.

References

Akilandaeaswari, B., Muthu, K., 2021. One-pot green synthesis of Au-Ag bimetallic nanoparticles from Lawsonia inermis seed extract and its catalytic reduction of environmental polluted methyl orange and 4-nitrophenol. J. Taiwan Inst. Chem. Eng. 127, 292–301.

Ali, S., Perveen, S., Ali, M., et al, 2020a. Bioinspired morphology-controlled silver nanoparticles for antimicrobial application. Mater. Sci. Eng. C 108, 110421.

Ali, S., Perveen, S., Ali, M., et al, 2020b. Nano-conjugates of Cefadroxil as efficient antibacterial agent against Staphylococcus aureus ATCC 11632. J. Clust. Sci. 31, 811–821.

Ali, S., Perveen, S., Shah, M.R., et al, 2020c. Bactericidal potentials of silver and gold nanoparticles stabilized with cefixime: a strategy against antibiotic-resistant bacteria. J. Nanopart. Res. 22, 1–12.

Ali, S., Chen, X., Shi, W., et al, 2021a. Recent advances in silver and gold nanoparticles-based colorimetric sensors for heavy metal ions detection: a review. Crit. Rev. Anal. Chem., 1–33

Ali, S., Iqbal, M., Naseer, A., et al, 2021b. State of the art of gold (Au) nanoparticles synthesis via green routes and applications: a review. Environ. Nanotechnol. Monit. Manage. 16, 100511.

Ali, S., Sharma, A.S., Ahmad, W., et al, 2021c. Noble metals based bimetallic and trimetallic nanoparticles: controlled synthesis, antimicrobial and anticancer applications. Crit. Rev. Anal. Chem. 51, 454–481.

Ali, S., Mansha, M., Baig, N., et al, 2022. Recent trends and future perspectives of emergent analytical techniques for mercury sensing in aquatic environments. Chem. Rec. e202100327.

Alp, E., İmamoğlu, R., Savacı, U., et al, 2021. Plasmon-enhanced photocatalytic and antibacterial activity of gold nanoparticles-decorated hematite nanostructures. J. Alloy. Compd. 852, 157021.

Al-Radadi, N.S., 2022. Microwave assisted green synthesis of Fe@Au Core-Shell NPs magnetic to enhance olive oil efficiency on eradication of Helicobacter pylori (Life preserver). Arab. J. Chem. 103685.

Amanulla, B., Perumal, K.N., Ramaraj, S.K., 2019. Chitosan functionalized gold nanoparticles assembled on sulphur doped graphitic carbon nitride as a new platform for colorimetric detection of trace Hg2+. Sens. Actuators B 281, 281–287.

Amico, D., Tassone, A., Pirrone, N., et al, 2022. Recent applications and novel strategies for mercury determination in environmental samples using microextraction-based approaches: a review. J. Hazard. Mater. 128823.

Amirjani, A., Haghshenas, D.F., 2018. Ag nanostructures as the surface plasmon resonance (SPR)- based sensors: a mechanistic study with an emphasis on heavy metallic ions detection. Sens. Actuators B 273, 1768–1779.

Árvay, J., Hauptvogl, M., Demková, L., et al, 2022. Mercury in scarletina bolete mushroom (Neoboletus luridiformis): Intake, spatial distribution in the fruiting body, accumulation ability and health risk assessment. Ecotoxicol. Environ. Saf. 232, 113235.

Azar, J., Yousef, M.H., El-Fawal, H.A., et al, 2021. Mercury and Alzheimer's disease: a look at the links and evidence. Metab. Brain Dis. 36, 361–374.

Bai, T., Wang, L., Wang, M., et al, 2022. Strategic synthesis of trimetallic Au@Ag–Pt nanorattles for ultrasensitive colorimetric detection in lateral flow immunoassay. Biosens. Bioelectron. 208, 114218.

Basu, N., Abass, K., Dietz, R., et al, 2022. The impact of mercury contamination on human health in the Arctic: A state of the science review. Sci. Total Environ. 154793.

Becerril-Castro, I.B., Calderon, I., Pazos-Perez, N., et al, 2022. Gold Nanostars: synthesis, optical and SERS analytical properties. Anal. Sens., e202200005

Bi, N., Zhang, Y., Xi, Y., et al, 2021. Colorimetric response of lysine-caped gold/silver alloy nanocomposites for mercury (II) ion detection. Colloids Surf. B Biointerfaces 205, 111846.

Bibi, G., Khan, S.R., Ali, S., et al, 2022. Role of capping agent in the synthesis of zinc–cobalt bimetallic nanoparticles and its application as catalyst and fuel additive. Appl. Nanosci., 1–13

Boeva, O., Kudinova, E., Vorakso, I., et al, 2022. Bimetallic gold-copper nanoparticles in the catalytic reaction of deuterium-hydrogen exchange: a synergistic effect. Int. J. Hydrogen Energy 47, 4759–4765.

Boken, J., Khurana, P., Thatai, S., et al, 2017. Plasmonic nanoparticles and their analytical applications: a review. Appl. Spectrosc. Rev. 52, 774–820.

Butmee, P., Mala, J., Damphathik, C., et al, 2021. A portable selective electrochemical sensor amplified with Fe_3O_4@Au-cysteamine-thymine acetic acid as conductive mediator for determination of mercuric ion. Talanta 221, 121669.

Chansuvarn, W., Tuntulani, T., Imyim, A., 2015. Colorimetric detection of mercury (II) based on gold nanoparticles, fluorescent gold nanoclusters and other gold-based nanomaterials. TrAC Trends Anal. Chem. 65, 83–96.

Chatterjee, S., Lou, X.-Y., Liang, F., et al, 2022. Surface-functionalized gold and silver nanoparticles for colorimetric and fluorescent sensing of metal ions and biomolecules. Coord. Chem. Rev. 459, 214461.

Chen, Z., Sun, Y., Shi, J., et al, 2022. Facile synthesis of Au@Ag core–shell nanorod with bimetallic synergistic effect for SERS detection of thiabendazole in fruit juice. Food Chem. 370, 131276.

Chen, X., Wei, M., Jiang, S., et al, 2019. Two growth mechanisms of thiol-capped gold nanoparticles controlled by ligand chemistry. Langmuir 35, 12130–12138.
Chen, R., Yi, G., Wu, S., et al, 2021. Controlled green synthesis of Au–Pt bimetallic nanoparticles using chlorogenic acid. Res. Chem. Intermed. 47, 4051–4066.
Chen, J.-K., Zhao, S.-M., Zhu, J., et al, 2020. Colorimetric determination and recycling of Hg^{2+} based on etching-induced morphology transformation from hollow AuAg nanocages to nanoboxes. J. Alloy. Compd. 828, 154392.
Cossa, D., Knoery, J., Bănaru, D., et al, 2022. Mediterranean mercury assessment 2022: an updated budget, health consequences, and research perspectives. Environ. Sci. Technol. 56, 3840–3862.
Crawley, J.W., Gow, I.E., Lawes, N., et al, 2022. Heterogeneous trimetallic nanoparticles as catalysts. Chem. Rev. 122, 6795–6849.
Da, Q., Gu, Y., Peng, X., et al, 2018. Colorimetric and visual detection of mercury (II) based on the suppression of the interaction of dithiothreitol with agar-stabilized silver-coated gold nanoparticles. Microchim. Acta 185, 1–9.
Dai, R., Deng, W., Hu, P., et al, 2018. One-pot synthesis of bovine serum albumin protected gold/silver bimetallic nanoclusters for ratiometric and visual detection of mercury. Microchem. J. 139, 1–8.
Deng, T.-S., Q. Zhang, M.-Z. Wei, et al., 2021. Control over the morphology and plasmonic properties of rod-like Au-Pd bimetallic nanostructures. J. Phys.: Conf. Ser., IOP Publishing.
Deng, S., Zhao, B., Xing, Y., et al, 2021a. Green synthesis of proanthocyanidins-functionalized Au/Ag bimetallic nanoparticles. Green Chem. Lett. Rev. 14, 45–50.
Dung, N.T., Linh, N.T., Chi, D.L., et al, 2021. Optical properties and stability of small hollow gold nanoparticles. RSC Adv. 11, 13458–13465.
Elayappan, V., Muthusamy, S., Mayakrishnan, G., et al, 2020. Ultrasonication–dry-based synthesis of gold nanoparticle-supported CuFe on rGO nanosheets for competent detection of biological molecules. Appl. Surf. Sci. 531, 147415.
Emam, H.E., El-Zawahry, M.M., Ahmed, H.B., 2017. One-pot fabrication of AgNPs, AuNPs and Ag-Au nano-alloy using cellulosic solid support for catalytic reduction application. Carbohydr. Polym. 166, 1–13.
Fan, T.-E., Liu, T.-D., Zheng, J.-W., et al, 2016. Structure and stability of Fe-Pt bimetallic nanoparticles: Initial structure, composition and shape effects. J. Alloy. Compd. 685, 1008–1015.
Fernandes, T., Fateixa, S., Ferro, M., et al, 2021. Colloidal dendritic nanostructures of gold and silver for SERS analysis of water pollutants. J. Mol. Liq. 337, 116608.
Fu, Q., Fu, C., Teng, L., et al, 2021. Rapid synthesis and growth process deconvolution of Au nanoflowers with ultrahigh catalytic activity based on microfluidics. J. Mater. Sci. 56, 6315–6326.
Ge, J., Chen, X., Yang, J., et al, 2021. Progress in electrochemiluminescence of nanoclusters: how to improve the quantum yield of nanoclusters. Analyst 146, 803–815.
Gebre, S.H., 2022. Synthesis and potential applications of trimetallic nanostructures. New J. Chem.
Goliaei, E.M., Seriani, N., 2019. Structure and Electronic Properties of Small Silver-Gold Clusters on Titania Photocatalysts for H2O2 Production: An Investigation with Density Functional Theory. J. Phys. Chem. C 123, 2855–2863.
Gu, Y., Jiang, Z., Ren, D., et al, 2021. Electrochemiluminescence sensor based on the target recognition-induced aggregation of sensing units for Hg2+ determination. Sens. Actuators B 337, 129821.
Gul, Z., Ullah, S., Khan, S., et al, 2022. Recent Progress in nanoparticles based sensors for the detection of Mercury (II) ions in environmental and biological samples. Crit. Rev. Anal. Chem., 1–17
Guo, Y., Sun, Q., Wu, F.G., et al, 2021. Polyphenol-Containing nanoparticles: synthesis, properties, and therapeutic delivery. Adv. Mater. 33, 2007356.
Hammami, I., Alabdallah, N.M., 2021. Gold nanoparticles: Synthesis properties and applications. J. King Saud Univ.-Sci. 33, 101560.
He, F., Ji, H., Feng, L., et al, 2021. Construction of thiol-capped ultrasmall Au–Bi bimetallic nanoparticles for x-ray CT imaging and enhanced antitumor therapy efficiency. Biomaterials 264, 120453.
He, M.-Q., Yu, Y.-L., Wang, J.-H., 2020. Biomolecule-tailored assembly and morphology of gold nanoparticles for LSPR applications. Nano Today 35, 101005.
Hlaváček, A., Farka, Z., Mickert, M.J., et al, 2022. Bioconjugates of photon-upconversion nanoparticles for cancer biomarker detection and imaging. Nat. Protoc., 1–45
Huang, J., Xiang, Y., Li, J., et al, 2021a. A novel electrochemiluminescence aptasensor based on copper-gold bimetallic nanoparticles and its applications. Biosens. Bioelectron. 194, 113601.
Huang, W., Zhu, J., Wang, M., et al, 2021b. Emerging mono-elemental bismuth nanostructures: controlled synthesis and their versatile applications. Adv. Funct. Mater. 31, 2007584.
Hyder, A., Buledi, J.A., Nawaz, M., et al, 2022. Identification of heavy metal ions from aqueous environment through gold, Silver and Copper Nanoparticles: an excellent colorimetric approach. Environ. Res. 205, 112475.
Ielo, I., Rando, G., Giacobello, F., et al, 2021. Synthesis, chemical–physical characterization, and biomedical applications of functional gold nanoparticles: a review. Molecules 26, 5823.
Irfan, M., Moniruzzaman, M., Ahmad, T., et al, 2022. Identifying the role of process conditions for synthesis of stable gold nanoparticles and insight detail of reaction mechanism. Inorganic Nano-Metal Chem. 52, 519–532.
Ismail, W.Z.W., Dawes, J.M., 2022. Synthesis and characterization of silver-gold bimetallic nanoparticles for random lasing. Nanomaterials 12, 607.
Jadoun, S., Arif, R., Jangid, N.K., et al, 2021. Green synthesis of nanoparticles using plant extracts: a review. Environ. Chem. Lett. 19, 355–374.
Jain, S., Manoj Kumaran, S., Satija, J., 2020. Bimetallic hollow nanostructures for colorimetric detection of picomolar level of mercury. J. Nanosci. Nanotechnol. 20, 991–998.
Jain, S., Satija, J., 2018. Investigation of bimetallic hollow nanoparticles for colorimetric detection of mercury. Int. Soc. Optics Photonics Nanophotonics VII.
Joseph, D., Kwak, C.H., Huh, Y.S., et al, 2019. Synthesis of AuAg@Ag core@ shell hollow cubic nanostructures as SERS substrates for attomolar chemical sensing. Sens. Actuators B 281, 471–477.
Kaviya, S., 2020. Synthesis, self-assembly, sensing methods and mechanism of bio-source facilitated nanomaterials: A review with future outlook. Nano-Struct. Nano-Objects. 23, 100498.
Khalaf, M.M., Abd El-Lateef, H.M., Mohamed, I.M., et al, 2021. Facile synthesis of gold-nanoparticles by different capping agents and their anticancer performance against liver cancer cells. Colloid Interface Sci. Commun. 44, 100482.
Khalil, M.M., Ismail, E.H., El-Magdoub, F., 2012. Biosynthesis of Au nanoparticles using olive leaf extract: 1st nano updates. Arab. J. Chem. 5, 431–437.
Khan, M., Al-Hamoud, K., Liaqat, Z., et al, 2020. Synthesis of au, ag, and au–ag bimetallic nanoparticles using pulicaria undulata extract and their catalytic activity for the reduction of 4-nitrophenol. Nanomaterials 10, 1885.
Khani, H., Abbasi, S., Yaraki, M.T., et al, 2022. A naked-eye colorimetric assay for detection of Hg2+ ions in real water samples based on gold nanoparticles-catalyzed clock reaction. J. Mol. Liq. 345, 118243.
Kluitmann, J., Zheng, X., Koehler, J.M., 2021. Tuning the morphology of bimetallic gold-platinum nanorods in a microflow synthesis. Colloids Surf. A Physicochem. Eng. Asp 626, 127085.

Kokilavani, S., Syed, A., Thomas, A.M., et al, 2020. Facile synthesis of Ag/Cu-cellulose nanocomposite for detection, photocatalysis and anti-microbial applications. Optik 220, 165218.
Kołątaj, K., Krajczewski, J., Kudelski, A., 2020. Plasmonic nanoparticles for environmental analysis. Environ. Chem. Lett. 18, 529–542.
Krishnan Sundarrajan, S., Pottail, L., 2021. Green synthesis of bimetallic Ag@ Au nanoparticles with aqueous fruit latex extract of Artocarpus heterophyllus and their synergistic medicinal efficacies. Appl. Nanosci. 11, 971–981.
Kukreti, S., Kaushik, M., 2021. Gold nanoclusters: An ultrasmall platform for multifaceted applications. Talanta 234, 122623.
Li, Y., Chen, L., Liang, S., et al, 2022b. Looping mercury cycle in global environmental-economic system modeling. Environ. Sci. Tech. 56, 2861–2879.
Li, Z., Li, M., Wang, X., et al, 2021b. The use of amino-based functional molecules for the controllable synthesis of noble-metal nanocrystals: a minireview. Nanoscale Adv. 3, 1813–1829.
Li, S.-H., Qi, M.-Y., Tang, Z.-R., et al, 2021a. Nanostructured metal phosphides: from controllable synthesis to sustainable catalysis. Chem. Soc. Rev. 50, 7539–7586.
Li, J.-J., Qin, Q.-X., Weng, G.-J., et al, 2022a. Improve the hole size-dependent refractive index sensitivity of Au–Ag nanocages by tuning the alloy composition. Plasmonics 17, 597–612.
Liebig, F., Sarhan, R.M., Prietzel, C., et al, 2018. Undulated gold nanoplatelet superstructures: in situ growth of hemispherical gold nanoparticles onto the surface of gold nanotriangles. Langmuir 34, 4584–4594.
Liu, Y., Chen, H., Zhu, N., et al, 2022a. Detection and remediation of mercury contaminated environment by nanotechnology: progress and challenges. Environ. Pollut. 293, 118557.
Liu, R., Duan, S., Bao, L., et al, 2020. Photonic crystal enhanced gold-silver nanoclusters fluorescent sensor for Hg^{2+} ion. Anal. Chim. Acta 1114, 50–57.
Liu, Y., Fang, Z., Kuai, L., et al, 2014. One-pot facile synthesis of reusable tremella-like M 1@ M 2@ M 1 (OH) 2 (M 1 = Co, Ni, M 2 = Pt/Pd, Pt, Pd and Au) three layers core–shell nanostructures as highly efficient catalysts. Nanoscale 6, 9791–9797.
Liu, X., Wang, A., Yang, X., et al, 2009. Synthesis of thermally stable and highly active bimetallic Au− Ag nanoparticles on inert supports. Chem. Mater. 21, 410–418.
Liu, T.-D., Xu, L.-Y., Shao, G.-F., et al, 2016. Structural optimization of Pt–Pd–Rh trimetallic nanoparticles using improved genetic algorithm. J. Alloy. Compd. 663, 466–473.
Liu, Y., Xu, Z., Zhu, S., et al, 2022b. Evaluation of synergistic effect of polyglycine functionalized gold/iron doped silver iodide for colorimetric detection, photocatalysis, drug delivery and bactericidal applications. J. Photochem. Photobiol. A Chem. 422, 113522.
Lu, F., 2022. Silver nanomaterials sensing of mercury ions in aqueous medium. Coord. Chem. Rev. 456, 214363.
Lu, Y., Zhong, J., Yao, G., et al, 2018. A label-free SERS approach to quantitative and selective detection of mercury (II) based on DNA aptamer-modified SiO_2@ Au core/shell nanoparticles. Sens. Actuators B 258, 365–372.
Ma, X., Gao, W., Du, F., et al, 2021. Rational design of electrochemiluminescent devices. Acc. Chem. Res. 54, 2936–2945.
Mathaweesansurn, A., Vittayakorn, N., Detsri, E., 2020. Highly sensitive and selective colorimetric sensor of Mercury (II) based on layer–by–layer deposition of gold/silver bimetallic nanoparticles. Molecules 25, 4443.
McLamore, E., Convertino, M., Ocsoy, I., et al, 2017. Biomimetic fractal nanometals as A transducer layer in electrochemical biosensing. World Sci. Semiconductor-Based Sensors, 35–67.
Mehta, V.N., Ghinaiya, N., Rohit, J.V., et al, 2022. Ligand chemistry of gold, silver and copper nanoparticles for visual read-out assay of pesticides: a review. TrAC Trends Anal. Chem. 116607.
Mitchell, M.J., Billingsley, M.M., Haley, R.M., et al, 2021. Engineering precision nanoparticles for drug delivery. Nat. Rev. Drug Discov. 20, 101–124.
Mitra, S., Chakraborty, A.J., Tareq, A.M., et al, 2022. Impact of heavy metals on the environment and human health: Novel therapeutic insights to counter the toxicity. J. King Saud Univ.-Sci. 101865.
Mukunzi, D., Habimana, J.D.D., Li, Z., et al, 2022. Mycotoxins detection: view in the lens of molecularly imprinted polymer and nanoparticles. Critical Rev. Food Sci. Nutr, 1–35.
Nanda, S.S., Hembram, K., Lee, J.-K., et al, 2019. Experimental and theoretical structural characterization of Cu–Au tripods for photothermal anticancer therapy. ACS Appl. Nano Mater. 2, 3735–3742.
Nieto-Argüello, A., Torres-Castro, A., Villaurrutia-Arenas, R., et al, 2021. Green synthesis and characterization of gold-based anisotropic nanostructures using bimetallic nanoparticles as seeds. Dalton Trans. 50, 16923–16928.
Nikolaou, P., Valenti, G., Paolucci, F., 2021. Nano-structured materials for the electrochemiluminescence signal enhancement. Electrochim. Acta 388, 138586.
Oladoye, P.O., Olowe, O.M., Asemoloye, M.D., 2022. Phytoremediation technology and food security impacts of heavy metal contaminated soils: a review of literature. Chemosphere 288, 132555.
Pandey, P.C., Mitra, M.D., Shukla, S., et al, 2021. Organotrialkoxysilane-Functionalized noble metal monometallic, bimetallic, and trimetallic nanoparticle mediated non-enzymatic sensing of glucose by resonance rayleigh scattering. Biosensors 11, 122.
Park, S.I., Song, H.-M., 2021. Several shapes of single crystalline gold nanomaterials prepared in the surfactant mixture of CTAB and pluronics. ACS Omega 6, 3625–3636.
Pawar, S., Teja, B.R., Nagarjuna, R., et al, 2019. Probing the surface composition effect of silver-gold alloy in SERS efficiency. Colloids Surf. A Physicochem. Eng. Asp 578, 123638.
Quyen, T.T.B., Su, W.-N., Chen, C.-H., et al, 2014. Novel Ag/Au/Pt trimetallic nanocages used with surface-enhanced Raman scattering for trace fluorescent dye detection. J. Mater. Chem. B 2, 5550–5557.
Ramos, R.M.C.R., Regulacio, M.D., 2021. Controllable synthesis of bimetallic nanostructures using biogenic reagents: a green perspective. ACS Omega 6, 7212–7228.
Rehman, Q., Rehman, K., Akash, M.S.H., 2021. Heavy metals and neurological disorders: from exposure to preventive interventions. Environmental contaminants and neurological disorders, Springer, pp. 69-87.
Rosi, N.L., Mirkin, C.A., 2005. Nanostructures in biodiagnostics. Chem. Rev. 105, 1547–1562.
Rycenga, M., Cobley, C.M., Zeng, J., et al, 2011. Controlling the synthesis and assembly of silver nanostructures for plasmonic applications. Chem. Rev. 111, 3669–3712.
Saeed, A., Akhtar, M., Zulfiqar, S., et al, 2022. Thiamine-functionalized silver–copper bimetallic nanoparticles-based electrochemical sensor for sensitive detection of anti-inflammatory drug 4-aminoantipyrine. Chem. Pap., 1–11
Saha, D., Gismondi, P., Kolasinski, K.W., et al, 2021. Fabrication of electrospun nanofiber composite of g-C3N4 and Au nanoparticles as plasmonic photocatalyst. Surf. Interfaces 26, 101367.
Salandari-Jolge, N., Ensafi, A.A., Rezaei, B., 2021. Ultra-sensitive electrochemical aptasensor based on zeolitic imidazolate framework-8 derived Ag/Au core-shell nanoparticles for mercury detection in water samples. Sens. Actuators B 331, 129426.
Sayadi, K., Akbarzadeh, F., Pourmardan, V., et al, 2021. Methods of green synthesis of Au NCs with emphasis on their morphology: a mini-review. Heliyon. 7, e07250.
Shah, M.R., Ali, S., Ateeq, M., et al, 2014. Morphological analysis of the antimicrobial action of silver and gold nanoparticles stabilized with ceftriaxone on Escherichia coli using atomic force microscopy. New J. Chem. 38, 5633–5640.

Shi, Y., Li, W., Feng, X., et al, 2021. Sensing of mercury ions in Porphyra by Copper@ Gold nanoclusters based ratiometric fluorescent aptasensor. Food Chem. 344, 128694.
Shrivastava, P., Jain, V., Nagpal, S., 2022. Nanoparticle intervention for heavy metal detection: a review. Environ. Nanotechnol. Monit. Manage. 17, 100667.
Si, Y., Bai, Y., Qin, X., et al, 2018. Alkyne–DNA-functionalized alloyed Au/Ag nanospheres for ratiometric surface-enhanced Raman scattering imaging assay of endonuclease activity in live cells. Anal. Chem. 90, 3898–3905.
Siddiqui, S., Nafady, A., El-Sagher, H.M., et al, 2019. Sub-ppt level voltammetric sensor for Hg^{2+} detection based on nafion stabilized l-cysteine-capped Au@ Ag core-shell nanoparticles. J. Solid State Electrochem. 23, 2073–2083.
Subhan, A., A.-H. I. Mourad and S. Das, 2022. Pulsed laser synthesis of bi-metallic nanoparticles for biomedical applications: a review. In: 2022 Advances in Science and Engineering Technology International Conferences (ASET), IEEE.
Tapia-Arellano, A., Gallardo-Toledo, E., Ortiz, C., et al, 2021. Functionalization with PEG/Angiopep-2 peptide to improve the delivery of gold nanoprisms to central nervous system: in vitro and in vivo studies. Mater. Sci. Eng. C 121, 111785.
Teng, H., Altaf, A.R., 2022. Elemental Mercury (Hg0) emission, hazards, and control: a brief review. J. Hazardous Mater. Adv. 100049.
Thangaswamy, S.J.K., Mir, M.A., Muthu, A., 2021. Green synthesis of mono and bimetallic alloy nanoparticles of gold and silver using aqueous extract of Chlorella acidophile for potential applications in sensors. Prep. Biochem. Biotech. 51, 1026–1035.
Tim, B., Błaszkiewicz, P., Kotkowiak, M., 2021. Recent advances in metallic nanoparticle assemblies for surface-enhanced spectroscopy. Int. J. Mol. Sci. 23, 291.
Ullah, I., Zhao, L., Hai, Y., et al, 2021. Metal elements and pesticides as risk factors for Parkinson's disease-A review. Toxicol. Rep. 8, 607–616.
Vilímová, I., Šišková, K., 2021. Distinctly Different Morphologies of Bimetallic Au-Ag Nanostructures and Their Application in Submicromolar SERS-Detection of Free Base Porphyrin. Nanomaterials 11, 2185.
Wang, B., Chen, M., Ding, L., et al, 2021a. Fish, rice, and human hair mercury concentrations and health risks in typical Hg-contaminated areas and fish-rich areas, China. Environ. Int. 154, 106561.
Wang, J., Ma, S., Ren, J., et al, 2018. Fluorescence enhancement of cysteine-rich protein-templated gold nanoclusters using silver (I) ions and its sensing application for mercury (II). Sens. Actuators B 267, 342–350.
Wang, J., Drelich, A.J., Hopkins, C.M., et al, 2022a. Gold nanoparticles in virus detection: Recent advances and potential considerations for SARS-CoV-2 testing development. Wiley Interdiscip. Rev. Nanomed. Nanobiotechnol. 14, e1754.
Wang, Y.-W., Liu, Q., Wang, L., et al, 2019. A colorimetric mercury (II) assay based on the Hg (II)-stimulated peroxidase mimicking activity of a nanocomposite prepared from graphitic carbon nitride and gold nanoparticles. Microchim. Acta 186, 1–8.
Wang, Z., Lu, Y., Pang, J., et al, 2020. Iodide-assisted silver nanoplates for colorimetric determination of chromium (III) and copper (II) via an aggregation/fusion/oxidation etching strategy. Microchim. Acta 187, 1–10.
Wang, W.-J., Lu, X.-Y., Kong, F.-Y., et al, 2022d. A reduced graphene oxide supported Au-Bi bimetallic nanoparticles as an enhanced sensing platform for simultaneous voltammetric determination of Pb (II) and Cd (II). Microchem. J. 175, 107078.
Wang, J., Ma, L.Q., Letcher, R., et al, 2022b. Biogeochemical cycle of mercury and controlling technologies: Publications in critical reviews in environmental science & technology in the period of 2017–2021. Crit. Rev. Environ. Sci. Technol., 1–6
Wang, J., Wang, W., Yang, L., et al, 2022c. Surface engineered bimetallic gold/silver nanoclusters for in situ imaging of mercury ions in living organisms. Anal. Bioanal. Chem., 1–10
Wang, Y., Wang, Y., Wang, F., et al, 2022e. Electrochemical aptasensor based on gold modified thiol graphene as sensing platform and gold-palladium modified zirconium metal-organic frameworks nanozyme as signal enhancer for ultrasensitive detection of mercury ions. J. Colloid Interface Sci. 606, 510–517.
Wang, J., Wu, J., Zhang, Y., et al, 2021b. Colorimetric and SERS dual-mode sensing of mercury (II) based on controllable etching of Au@ Ag core/shell nanoparticles. Sens. Actuators B 330, 129364.
Xie, H., Niu, Y., Deng, Y., et al, 2021. Electrochemical aptamer sensor for highly sensitive detection of mercury ion with Au/Pt@ carbon nanofiber-modified electrode. J. Chin. Chem. Soc. 68, 114–120.
Xie, H., Wei, X., Zhao, J., et al, 2022. Size characterization of nanomaterials in environmental and biological matrices through non-electron microscopic techniques. Sci. Total Environ. 155399.
Xing, T.-Y., Zhao, J., Weng, G.-J., et al, 2018. Synthesis of dual-functional Ag/Au nanoparticles based on the decreased cavitating rate under alkaline conditions and the colorimetric detection of mercury (ii) and lead (ii). J. Mater. Chem. C 6, 7557–7567.
Yao, J.-Y., Santos, E.B., 2020. An improved method for fabrication of patterned composites made of silver or gold nanoparticles embedded in PDMS structures and their colorimetric characterization. Nano-Structures & Nano-Objects. 23, 100510.
Yu, F., Luo, P., Chen, Y., et al, 2021. The synthesis of novel fluorescent bimetal nanoclusters for aqueous mercury detection based on aggregation-induced quenching. Anal. Methods 13, 2575–2585.
Yu, L., Song, Z., Peng, J., et al, 2020. Progress of gold nanomaterials for colorimetric sensing based on different strategies. TrAC Trends Anal. Chem. 127, 115880.
Zaheer, T., 2021. Fabrication of Ultra-Pure Anisotropic Nanoparticles, Spectroscopic Studies and Biological Applications. Nanomaterials for Spectroscopic Applications, Jenny Stanford Publishing: 173-190.
Zhai, Q., Xing, H., Zhang, X., et al, 2017. Enhanced electrochemiluminescence behavior of gold–silver bimetallic nanoclusters and its sensing application for mercury (II). Anal. Chem. 89, 7788–7794.
Zhang, M., Guo, X., 2022. Gold/platinum bimetallic nanomaterials for immunoassay and immunosensing. Coord. Chem. Rev. 465, 214578.
Zhang, N., Qiu, Y., Sun, H., et al, 2021. Substrate-Assisted Encapsulation of Pd-Fe Bimetal Nanoparticles on Functionalized Silica Nanotubes for Catalytic Hydrogenation of Nitroarenes and Azo Dyes. ACS Appl. Nano Mater. 4, 5854–5863.
Zhang, L., Wang, E., 2014. Metal nanoclusters: new fluorescent probes for sensors and bioimaging. Nano Today 9, 132–157.
Zhang, J., Zhu, K., Hao, H., et al, 2019. A novel chitosan modified Au@ Ag core-shell nanoparticles sensor for naked-eye detection of Hg^{2+}. Mater. Res. Express 6, 125045.
Zhao, J., Xu, N., Yang, X., et al, 2022. The roles of gold nanoparticles in the detection of amyloid-β peptide for Alzheimer's disease. Colloid Interface Sci. Commun. 46, 100579.
Zhou, T., Li, M., Li, N., et al, 2022. Ultrasensitive electrochemical sensor for mercury ion detection based on molybdenum selenide and Au nanoparticles via thymine–Hg 2+–thymine coordination. Anal. Methods.
Zhu, J., Chang, H., Li, J.-J., et al, 2018. Using silicon-coated gold nanoparticles to enhance the fluorescence of CdTe quantum dot and improve the sensing ability of mercury (II). Spectrochim. Acta A Mol. Biomol. Spectrosc. 188, 170–178.
Zhu, J., Jia, T.-T., Li, J.-J., et al, 2019. Plasmonic spectral determination of Hg (II) based on surface etching of Au-Ag core-shell triangular nanoplates: from spectrum peak to dip. Spectrochim. Acta A Mol. Biomol. Spectrosc. 207, 337–347.
Zhu, Q., Zhang, W., Cai, J., et al, 2022. Morphology-controlled synthesis of gold nanoparticles with chitosan for catalytic reduction of nitrophenol. Colloids Surf A Physicochem Eng Asp 640, 128471.